This is the peer reviewed version of the following article: Scarciglia, F., Critelli, S., Borrelli, L., Coniglio, S., Muto, F., Perri, F., 2016. Weathering profiles in granitoid rocks of the Sila Massif uplands, Calabria, southern Italy: new insights into their formation processes and rates. Sed. Geol. 336, 46–67, which has been published in final form at: http://dx.doi.org/10.1016/j.sedgeo.2016.01.015

Weathering profiles in granitoid rocks of the Sila Massif uplands, Calabria, southern Italy: new insights into their formation processes and rates

Fabio Scarciglia [a,*], Salvatore Critelli [a], Luigi Borrelli [b], Sabrina Coniglio [a,c], Francesco Muto [a], Francesco Perri [a]

[a] *Dipartimento di Biologia, Ecologia e Scienze della Terra (DiBEST), Università della Calabria, Via P. Bucci – Cubo 15B, 87036 Arcavacata di Rende (CS), Italy*

[b] *Istituto di Ricerca per la Protezione Idrogeologica (IRPI), Consiglio Nazionale delle Ricerche (CNR), Via Cavour 6, 87036 Rende (CS), Italy*

[c] *Ente Parco Nazionale della Sila, Via Nazionale, 87055 Lorica, San Giovanni in Fiore (CS), Italy*

[*] Corresponding author: E-mail address: fabio.scarciglia@unical.it (F. Scarciglia)

Abstract

In this paper we characterized several weathering profiles developed on granitoid rocks in the Sila Massif upland (Calabria, southern Italy), integrating detailed macro- and micromorphological observations with physico-mechanical field tests and petrographic, mineralogical and geochemical analyses. We focused our attention on the main weathering and pedogenetic processes, trying to understand apparent discrepancies between weathering grade classes based on field description and geomechanical properties, and two common weathering indices, such as the micropetrographic index (Ip) and the chemical index of alteration (CIA). Our results showed that sericite on plagioclase and biotite chloritization, that represent inherited features formed during late-stage hydrothermal alteration of granitoid rocks, may cause an overestimation of the real degree of weathering of primary mineral grains under meteoric conditions, especially in lower weathering grade classes. Moreover, the frequent identification of Fe-Mn oxides and clay coatings of illuvial origin (rather than or in addition to those formed in situ), both at the macro- and microscale, may also explain an overestimation of the weathering degree with respect to field-based classifications. Finally, some apparent inconsistencies between field geomechanical responses and chemical weathering were interpreted as related to physical weathering processes (cryoclastism and thermoclastism), that lead to rock breakdown even when chemical weathering is not well developed. Hence, our study showed

that particular caution is needed for evaluating weathering grades, because traditional field and geochemical-petrographic tools may be biased by inherited hydrothermal alteration, physical weathering and illuvial processes. On the basis of chronological constraints to soil formation obtained from a 42 ka-old volcanic input (mixed to granite parent materials) detected in the soil cover of the Sila Massif upland, a first attempt to estimate soil formation rates was achieved for different depths of corresponding weathering profile zones. Soil formation rates ranged from 0.01-0.07 mm a^{-1} for A and Bw horizons (weathering class VI) to 0.04-0.36 mm a^{-1} for the underlying saprolite (C and Cr layers; class V). By comparing these results with the corresponding erosion rates available in the literature for the study area, that range from <0.01-0.05 to 0.10-0.21 mm a^{-1}, we suggest that the upland landscape of the Sila Massif is close to steady-state conditions between weathering and erosive processes.

Keywords: *granitoid rocks; weathering profiles; weathering grades; in situ weathering; illuvial processes; soil formation rates*

1. Introduction

Weathering studies cover a quite large variety of topics, often accomplished by applying multi- or trans-disciplinary approaches, in turn involving multi-scale and multi-analytical procedures. Available literature spans from morphological and visual investigations (e.g., Bourke and Viles, 2007) to climatic geomorphology and landscape evolution (Dixon and Thorn, 2005; Dixon, 2013; Migoń, 2013b; Pope, 2013b; Migoń and Vieira, 2014), to petrographic, mineralogical, micromorphological and/or geochemical approaches (e.g., Critelli et al., 1991; Blum and Erel, 1997; Kretzschmar et al., 1997; Taboada and García, 1999a, 1999b; Le Pera et al., 2001a, 2001b; Sequeira Braga et al., 2002; Zauyah et al., 2010; Mavris et al., 2012; Campodonico et al., 2014), hydrological or geotechnical characterization of weathering profiles (Chigira and Yokoyama, 2005; Pellegrino and Prestininzi, 2007; Heidari et al., 2013) or modeling of weathering processes (Buss et al., 2008; Apollaro et al., 2009, 2013a, 2013b; Perri et al., 2015), up to estimation of ages of regolith mantles and weathering rates (Migoń and Lidmar-Bergström, 2002; Heimsath, 2006; Dosseto et al., 2008; Dixon et al., 2009; Chabaux et al., 2013; Migoń, 2013b), implications for sediment generation and composition (Johnsson, 1993; Arribas et al., 2000; Critelli et al., 2003; Le Pera and Arribas, 2003; Caracciolo et al., 2012; Pope, 2013a), etc. Among these approaches, several papers aimed at defining a classification of weathering grades based on geochemical parameters and ratios (Nesbitt and Young, 1982; Harnois, 1988; Birkeland, 1999; Darmody et al., 2005), petrographic indices (Lumb, 1962;

Irfan and Dearman, 1978; Palomares and Arribas, 1993) and qualitative, visual observations coupled with physico-mechanical tests (Ruxton and Berry, 1957; GEO, 1988; Gullà and Matano, 1997; Arikan and Aydin, 2012; Perri et al., 2012a; Borrelli et al., 2012b, 2014). Although several papers highlight a general accordance between weathering grade classes and increasing or decreasing trends of weathering ratios and indices (e.g., Nesbitt et al., 1997; Arel and Tugrul, 2001; Haskins, 2006), in some cases a deeper examination of the analytical results suggests that these features are not always strictly coupled (Kirschbaum et al., 2005; Gong et al., 2013; Chiu and Ng, 2014; Perri et al., 2015). In this work we aimed at exploring apparent discrepancies between weathering grade classes (based on field description and geomechanical properties) and some petrographic or chemical weathering indices. We focused on a more detailed description of weathering features at the macro- and microscales, giving an emphasis on weathering and pedogenetic processes, including both in situ chemical weathering and translocation of secondary products. Moreover, a first attempt to estimate soil formation rates is proposed in this work, as weathered, loose and mobile materials represent potential sources of sediments entering the drainage river system. Hence, these results were discussed in the light of their interplay with erosion rates. To these purposes, novel morphological, petrographic, mineralogical and geochemical data on weathering profiles from large areas of the Sila Massif (Calabria, southern Italy) were integrated with some published results. The Sila upland represents a key site to a deeper understanding of weathering processes on plutonic rocks in the central Mediterranean basin, as a consequence of a combination of peculiar geolithological, tectonic, geomorphological and climatic factors, and their interplay with a number of morphodynamic processes (e.g., Le Pera and Sorriso-Valvo, 2000b; Scarciglia et al., 2005b, 2007; Borrelli et al., 2007; Terranova et al., 2007, 2009).

2. Materials and methods

2.1 Geological and geomorphological setting of the study area

The study area is located in the Sila Massif upland (Calabria, southern Italy) (Fig. 1), that represents part of an orogenic segment (Calabrian Arc) located between the Calabrian-Lucanian Apennines and the Maghrebian Chain, formed during the Paleogene, and overthrusted during the Miocene over the Apennine Chain (e.g., Bonardi et al., 2001). The bulk of the relief consists of a Paleozoic crystalline basement, which includes medium- to high-grade metamorphic rocks (amphibolite to granulite facies) intruded by late Hercynian granitoids (Sila batholith), and forming the highest tectonic units of the fold-and-thrust belt of southern Italy (e.g., Messina et al., 2004). The Sila batholith consists of

tonalite, monzogranite and minor granodiorite (Messina et al., 1991; Liotta et al., 2008), discontinuously covered by unmetamorphosed Mesozoic to Cenozoic sedimentary rocks (e.g., Van Dijk et al., 2000; Critelli et al., 2011, 2013).

Since the Miocene the Sila Massif margins were covered by terrigenous sedimentary successions (Van Dijk et al., 2000; Barone et al., 2008; Zecchin et al., 2012; Muto et al., 2014; Perri et al., 2012b, 2014) and experienced brittle deformation. Strike-slip tectonics displaced the Sila Massif rocks and the Neogene-Quaternary basins (Critelli and Le Pera, 1995, 1998; Barone et al., 2008; Critelli et al., 2013; Fabbricatore et al., 2014), developing transpressional and transtensional blocks. Starting from the Neogene the ancient, thin, flat-lying thrust belt of the Calabrian Arc and of the Sila Massif, were dissected and displaced by the intersection of regional NW-SE and N-S fault systems (Fig. 2A). The first system is characterized by inherited, early Pleistocene regional, left-lateral strike-slip faults, reactivated as normal with left-lateral component of displacement during the middle-upper Pleistocene (Van Dijk et al., 2000; Spina et al., 2007; Tansi et al., 2007; Corbi et al., 2009; Tripodi et al., 2013). Very wide fault damage zones occur, with an occasional thick argillification of the fault core (Borrelli et al., 2015b). The Sila Massif shows present-day tectonic activity, as indicated by an intense seismicity along the western piedmont zone (Tortorici et al., 1995) and the major NW-SE transversal fault system (Spina et al., 2007).

The geomorphological evolution of the Sila Massif is mainly related to a multiphase tectonic uplift alternated to prolonged phases of relative geomorphological stability (Olivetti et al., 2012). During stable geomorphic conditions or slowly lowering base level a gently rolling landscape was shaped across the crystalline basement and in particular the granitoid rocks (planation surfaces of Pliocene-Pleistocene ages; e.g., Molin et al., 2004, 2012). The flat topography favored intense chemical weathering processes, resulting in deep weathering profiles. The intervening tectonic events progressively displaced this low-relief landscape and uplifted the fragmented blocks at elevations between about 1000 and 1700 m a.s.l. on top of the massif. Uplift started at a slow rate in the late Tertiary and underwent a strong acceleration in the middle Pleistocene (e.g., Westaway, 1993; Olivetti et al., 2012). The main scarps and drainage network, as well as river longitudinal profiles, appear strongly controlled by all the major NW-SE and N-S tectonic lineaments (Molin et al., 2004, 2012; Borrelli et al., 2015a, 2015b), that mutually intersect to create a complex, chessboard-like morphotectonic pattern. The deepening of the hydrographic system, caused by the tectonically-driven high local relief mainly along the steep massif flanks (cf. Martino et al., 2009; Schiattarella et al., 2013), favored a severe mechanical erosion of source rocks from the weathered mantles (e.g., Matano and Di Nocera, 1999; Le Pera et al., 2001a, 2001b; Scarciglia, 2015). This is confirmed by a rapid and short transport through the drainage system indicated by compositionally immature fluvial sands

in the main rivers draining the Sila Massif (Le Pera and Sorriso-Valvo, 2000b; Le Pera et al., 2001a; Critelli and Le Pera, 2002; Scarciglia et al., 2007).

The granitoid rocks, affected by intense and deep weathering processes, outcrop in the Sila Massif for an area of about 870 km^2. A small scale map of the weathering grade of these rocks obtained by Borrelli et al. (2012a) (Fig. 2B) allows a general overview of the intensity and spatial distribution of three macro-classes of weathering: macro-class A (soil-like material), that includes classes VI (soil and colluvium) and class V (completely weathered rock); macro-class B (weak rock), that includes class IV (highly weathered rock) and class III (moderately weathered rock); macro-class C (hard rock), that includes class II (slightly weathered rock) and class I (fresh rock) (Fig. 2B). The macro-class A terrains (ca. 63% of the whole area occupied by granitoids) widely crop out at the top of the paleosurface in the summit areas, where they are covered with both Pleistocene lacustrine deposits hosted in morphotectonic depressions (Scarciglia et al., 2005a, 2005b) and Holocene alluvial and/or colluvial deposits, these latter widespread in topographic lows or morphological hollows. At some sites, such as near Cecita Lake, Silvana Mansio and Lagarò, macro-class A is tens of meters thick (Fig. 2B). The macro-class B (about 32% of the granitoid surface) crops out prevalently along the slopes, whereas macro-class A (ca. 5% of the entire granitoid area) crops out only along the deeply incised main streams (e.g., Mucone, Trionto and Neto rivers; Fig. 2B). Rocks are cross-cut by a complex fracture pattern related to regional and local-scale faults and fault zones developed during ancient and recent tectonic phases (cf. Scarciglia et al., 2005a, 2007; Borrelli et al., 2014, 2015a, 2015b). This pattern consists of two main fault systems oriented N-S and NW (Fig. 2B). The first exhibits a prevalent normal kinematics and is responsible of the uplifted and downthrown blocks (e.g., Cecita Lake and San Giovanni fault system). The footwall rocks are characterized by fresher rocks belonging to macro-classes B and C (Fig. 2B). Rocks belonging to the widespread macro-class A outcrop along the hanging-wall block. The NW fault system is characterized by longer segments that cross the entire Sila Massif. These fault zones, consist of wide fault gouges and breccias, and undergo watercourse erosion and valley downcutting, that expose to daylight the rocks of macro-classes B and C (e.g., in the area between San Giovanni in Fiore and Ampollino-Arvo Lakes). The peculiar geological and structural features, coupled with the typical mountainous Mediterranean climate of the Sila Massif, strongly controlled the response of the upland landforms to the major morphogenetic processes, where a range of physical and chemical weathering processes on granitoid rocks contributed to landscape evolution (e.g., Le Pera and Sorriso-Valvo, 2000b; Scarciglia et al. 2005a, 2005b, 2007; Borrelli et al., 2012c, 2014; Perri et al., 2015). The main erosional landforms consist of wide boulder fields exposed on the flat to gently rolling planation surfaces, aligned along ridges or grouped as castellated piles on residual hilly reliefs of the summit landscape. Also tors and

bornhardts often occur on top of ridges and steep slopes close to the upper reaches of stream incisions (Le Pera and Sorriso-Valvo, 2000a; Scarciglia et al., 2005a, 2007; Scarciglia, 2015).

2.2 Field work and laboratory analyses

About 90 weathering profiles developed on granitoid rocks located in the Sila Massif highlands were described in the field on natural and artificial cut slopes to investigate their main weathering features and related processes. These profiles are representative of the mountainous landscapes comprised in the neighborhood of Acri, Longobucco, Camigliatello, Silvana Mansio and San Giovanni in Fiore villages (Fig. 2). They were carefully characterized following the methodology proposed by Gullà and Matano (1997), to classify the weathering front into six different classes from the fresh/unweathered bedrock (class I) to completely weathered rock, soil and colluvial material (class VI) (Table 1). The field survey was based on a detailed description of morphological features of the rock (fabric, color, texture and any other weathering features) and on its physical (resistance to rupture, scratching and indentation) and acoustic responses to solicitations with a geological hammer, coupled with evaluation of the elastic rebound (compressive strength) of rock masses on representative samples for each weathering class using a Schmidt hammer (sclerometer). Selected samples for each weathering class were also collected for laboratory analyses. These samples were thin-sectioned for detailed microfabric and minero-petrographic description under a polarizing optical microscope and by scanning electron microscopy (SEM) coupled with energy dispersive spectrometry (EDS) microprobe. Qualitative petrographic observations were carried out on 40 thin sections. Quantitative data were obtained by point counting on 29 selected thin sections, calculating the micropetrographic index (Ip) proposed by Irfan and Dearman (1978). This index is defined as a ratio among unweathered primary minerals and weathered minerals including secondary (neoformed) phases together with microcracks and voids, and thus tends to decrease as far as weathering goes on. SEM-EDS analyses were performed on about 30 bulk samples, focused on identification of the major weathering microtextures and neogenic products based on major element concentrations (e.g., Mulyanto et al., 1999; Scarciglia et al., 2011). A FEI Quanta 200 scanning electron microscope equipped with an EDAX Genesis 4000 system was used at DiBEST, Università della Calabria (Italy). Furthermore, these samples were prepared by milling to a fine grained powder in an agate mill for geochemical analyses. Concentrations of major and some trace elements (such as Nb, Zr, Y, Sr, Ba, Ni, Co, V, Cu, Zn, Pb, La, Ce) were obtained by X-ray fluorescence spectrometry (XRF) for rock samples classified with varying weathering grades, and compared with additional compositional data available in the literature (Messina et al., 1991) for more than 60 samples. Compositional analyses

were performed with a Bruker S8 Tiger spectrometer (DiBEST, Università della Calabria, Italy) on pressed powder disks of whole-rock samples and compared to international reference rock standards of the USGS (United States Geological Survey). Total loss on ignition (L.O.I.) was determined after heating the samples for three hours at 900 °C. The chemical index of alteration (CIA) proposed by Nesbitt and Young (1982) was calculated as the ratio: $Al_2O_3/(Al_2O_3 + CaO + Na_2O + K_2O) \times 100$, where CaO represents the Ca content in silicate minerals only.

A first estimation of soil formation rates (in terms of net lowering of the weathering/pedogenetic front from the topographic surface; e.g., Egli et al., 2014) was achieved by dividing various recurrent depths of weathering profile zones measured in the field on the most stable landforms of the summit landscape (where the soil cover is better preserved and thus virtually unaffected – or less affected~~, at least –~~ by surface erosion), by time of exposure of fresh rock to weathering and soil formation processes. This time interval was estimated using age constraints to soil development available from the literature and other field-based controls in the area between Silvana Mansio and San Giovanni in Fiore sites.

3. Results

3.1 Field features

The granitoid rocks exposed in the study area display a general trend of increase of the degree of weathering from top to bottom, as expected as a consequence of the downward deepening of the weathering front. However, the physical and chemical weathering pattern is often more complex, as controlled by the juxtaposition of varying lithological units and tectonic discontinuities affecting the substrate, such as changes in rock mineral assemblages, fabric or texture, fault planes, shear zones and aplite dikes (Fig. 3A, B, C). These features also affect the type of debris removed by gravity from the weathering profiles, which ranges from large angular/subangular blocks to rounded corestones and boulders up to loose, granular material consisting of small polymineral and monomineralic grains (Fig. 3D).

The most recurrent weathering grades identified in the field are comprised between class II (slightly weathered) to class VI (completely weathered), that commonly occur within weathering profiles in the range of ca. 4 to 8 m depths or more (Fig. 4A, B, C), and rarely reach 20-25 m up to about 50 m (cf. Le Pera and Sorriso-Valvo, 2000a; Borrelli et al., 2015a; Perri et al., 2015; Scarciglia, 2015). Transitional grades between subsequent weathering classes are very frequent. Class I (fresh, unweathered, hard rock) is virtually absent (not exposed). The only rock outcrops of class I are the

spheroidal boulders exhumed at the topographic surface, that in the area between Silvana Mansio and san Giovanni in Fiore form wide boulder fields. They frequently overlie weathering profiles ranging from class II to V or VI (Fig. 5A, B). However, the outer portion of these boulders often appears weakly weathered (class II), showing biotite oxidation and flaking, concentric laminar sheeting (surface exfoliation) and microfracturing, large block spalling and/or lichen colonization (Fig. 5C, D) (cf. Le Pera and Sorriso-Valvo, 2000a; Scarciglia et al., 2005a, 2007, 2012). Very slightly weathered rock masses with a transitional weathering grade (class I-II) are more common. They are mainly affected by physical breakage patterns, with deep fractures (some decimeters to meters in length) isolating large, angular blocks. An increasing degree of weathering of primary minerals appears from class I-II to VI, with a progressive loss of transparency of quartz grains, translucency of K-feldspar and plagioclase, exfoliation and oxidation of micas. This behavior is accompanied by a progressive smoothing of rock edges (up to concentric, spheroidal patterns isolating weathered corestones in the saprolite) (Fig. 6A) and/or an increase in rock microfractures up to a centimetric scale (Fig. 6B). Also rock strength (resistance to rupture, scratching and indentation, and elastic rebound) declines accordingly, from hard rock (classes I-II) to weak rock (III and IV), to soft rock (class V) and soil (class VI) or coarse-textured single-grain debris. Class VI includes proper soil horizons (A and/or Bw), that are on average 30-50 cm and 60-100 cm deep (Fig. 6C, D), respectively, with deeper and more horizonated soil profiles occurring under long-lived forest stands and flat landforms. Greater depths of about 5-6 m occur in topographic depressions and along footslope belts, where soil materials are affected by strong colluvial processes, often include angular to subangular rock clasts (ranging in size from 2-3 to 8-10 cm) and/or are buried by younger slope deposits. The soil horizons show dominant subangular blocky structure of pedogenic origin (coupled with crumby/granular aggregates in the topsoil) and (dark) brown (A) to yellowish brown (Bw) colors. On crests and steep slopes the soil profile is very shallow and often consists of a centimeter to decimeter-thick topsoil directly on the saprolite/bedrock, as a consequence of severe erosion rejuvenating the weathering front. It may completely lack, so that the bare rock with varying degree of weathering is exposed at the ground surface. The underlying saprolite (C and Cr layers) commonly reaches 120-150 cm to 3-5 m depth and corresponds to class V. It is mainly soft and friable, easy to dug with hand tools and prone to granular (grain-by-grain) disintegration (e.g., Butzer, 1976) or arenization (Power and Smith, 1994; Teeuw et al., 1994) upon small pressure, but still retains some original rock structure and fabric, with a lower bulk density. It usually appears pervasively weathered, with a (dark) brown to reddish-brown and brownish- to (reddish-)yellow, iron-stained and clay-rich groundmass, which includes whitish relicts of the original rock (Fig. 7A). The intermediate weathering grades represent moderately (class III) to highly weathered (class IV) rocks. They consist of rock masses displaying the main texture and

fabric of the fresh rock, with a pervasive to almost complete change in color, respectively, from (reddish-) to (brownish-)yellow, where a clay- and iron-oxyhydroxide matrix developed. Rocks belonging to classes II to IV (and especially III and III-IV) very often exhibit occasional to very abundant, spotted to extensive, (reddish-)yellow to yellowish-red and (very) dark brown to black, Fe-Mn-oxide/hydroxide staining (Fig. 7B), that sporadically also occur in class V samples, as well as dark (reddish-)brown clay coatings of illuvial origin, on fracture surfaces (Fig. 7C, D). Many weathering profiles are commonly cross-cut by a few centimeter- to decimeter-thick, white to pale yellow, aplite dykes of different chemical and mineralogical composition and finer texture than surrounding granitoid rocks. They are usually less weathered than the host rock, and undergo much more physical fragmentation than chemical weathering, often remaining as relatively preserved, continuous hard rock intrusions (weathering grade classes I-II to III) (Fig. 3C) or discontinuous block alignments within the surrounding, soft saprolitic mass. Their surfaces are sometimes iron-stained or covered by illuvial clay coatings. Most of the rocks described in the profiles show a coarse to very coarse texture, even in proper soil horizons (A, Bw and C) where the clay fraction never exceeds 18%, as clearly documented by previous laboratory measurements (e.g., Scarciglia et al., 2005a, 2005b, 2008; Pelle et al., 2013b; Borrelli et al., 2014).

A number of weathering profiles in the area between Silvana Mansio and San Giovanni in Fiore are exposed below spheroidal boulders of class I-II exhumed at the topographic surface, with the non-exhumed counterparts of weathered rocks always affected by a lesser degree of rounding and/or a more intense weathering.

3.2 Petrographic observations, Ip index and SEM-EDS analyses

The mineral assemblage of the studied rocks consists of prevalent quartz or K-feldspar (with common microcline, that in some samples hugely dominates over quartz and plagioclase grains), followed by plagioclase, biotite (Fig. 8A, B) and minor amounts of chlorite and/or muscovite. Epidote, apatite, zircon, amphibole and/or opaque minerals occur among accessory phases. Alkali feldspar and plagioclase crystals often displayed twinning and/or concentric zonation. Class I-II and II samples in thin sections evidenced occasional rock microcracks, very poor biotite oxidation or argillification with partial flaking and bending along outer edges of cleavage planes, varying amounts of sericite mica flakes mainly in the core of plagioclase, (Fig. 8C), occasional surface pitting of feldspar. Rocks classified as classes II, II-III and III-IV display very rare to extensive rock fractures, a higher (poor to moderate and occasionally severe) degree of weathering of biotite, that is partly split into two or more lamellae, with inter- and intra-granular cracks radiating towards surrounding mineral grains and

a clear migration of Fe(-Mn)-oxides (and more rarely clays) into these cracks (Fig. 8D-H). A similar behavior is observed on chlorite crystals (and chloritized biotite), also affected by local oxidation and clay neogenesis. Alkali feldspar grains very rarely appear weakly sericitized and show scanty etch pits, sometimes concentrated along parallel lines. Plagioclases may show early to diffuse clay neoformation and etching, in places with a differential, concentric pattern controlled by their compositional zoning and frequent sericitization of the core, up to complete pseudomorphs. More rarely plagioclase grains exhibit an almost pervasive growth of sericite, especially in the Silvana Mansio area. Conversely, in a few samples, both feldspar and plagioclase appear very poorly weathered. Some samples of classes III to IV or their transition also exhibit some surface corrosion of quartz grains, as well as rock fractures frequently infilled with illuvial clay coatings and/or iron oxyhydroxides (Fig. 9A, B), and rare opaque, iron-stained, clayey matrix patches with small anisotropic domains observed in crossed polarized light. In some cases granitoid samples belonging to class II-III exhibit more intense and diffuse chemical weathering than those classified as III-IV. Weathering grade classes V and VI are characterized by an overall diffuse breakage pattern of rock with inter- and intra-grain fractures, moderately to extremely weathered biotite (exfoliated, cleaved, oxidized and argillified up to frequent or occasional, unrecognizable pseudomorphous grains and matrix patches) (Fig. 9C, D), iron-stained or clay-coated cracks especially close to weathered biotite, very weathered plagioclase and feldspar, affected by common to poor sericitization, respectively-and by diffuse etch pits and/or clay neogenesis (Fig. 9E, F), sparse surface pitting of quartz (Fig. 9G, H), and large matrix zones rich in clay and Fe-oxides separating mineral grains or rock fragments.

The micropetrographic index Ip of the selected samples exhibit an overall decreasing trend from class I-II to V-VI, as expected. However, a few samples of classes V and V-VI show higher values than some less weathered classes, such as transitional III-IV and IV-V (Table 2).

SEM analyses on bulk samples confirmed the main weathering patterns of primary minerals evidenced under the optical microscope (Figs. 10A-D and 11A-D). In addition, microprobe compositional data of the weathered parts of these mineral grains and of illuvial coatings evidenced the occurrence of varying groups of phyllosilicate clays as secondary products, in places coupled with local Fe- and/or Mn-oxides. In particular, 1:1 clay minerals (such as kaolinite and/or halloysite) were identified where Si/Al ratios were close to 1 and associated to generally very poor amounts of other cations, and 2:1 clays (including vermiculite, illite and/or smectite) where greater Si/Al ratios generally around 2 were detected, along with varying percentages of Mg, Fe, K, Ca and/or Na.

3.3 Geochemical data

The results of major and trace element analysis were grouped into weathering grade classes obtained in the field, including transitional classes (see section 3.1), and the mean value was considered for each class (Tables 3 and 4). Compositional data of rock samples from the literature were considered as potentially transitional class I(-II), because of the lack of 'pure' class I weathering grade. Classes represented by only one sample (II-III and IV-V) were not included in the final dataset, which finally embraces the following groups: I(-II) (Messina et al., 1991), I-II, II, III, III-IV, IV, V and VI. For some chemical species an overall trend of increase (e.g., for Al_2O_3) or decrease (e.g., SiO_2) can be observed with increasing weathering grade, though some classes (commonly III, III-IV and/or IV) do not fit this behavior. A similar increase is shown by the CIA index, where only class III does not match the main trend (Fig. 12A). However, irregular patterns from class I-II to VI are more often detected for both major oxides and trace elements. Some species (e.g., CaO, K_2O and Sr) exhibit varying trends, with an initial decline followed by an increase in concentration from lower to higher grade weathering classes or vice versa. A number of molar ratios between elements with different relative mobility display at least partly similar trends to those of single chemical species and sometimes irregular patterns (Figs. 12-16). In particular, many of them commonly show important peaks for the weathering grade class III-IV.

3.4 Chronological constraints and soil formation rates

Previous studies indicated a partial contribution of fine volcanic ash to pedogenesis (in addition to granitoid parent materials) in the soil cover of the Sila upland landscape (Scarciglia et al., 2005b, 2008; Pelle et al., 2013b; Scarciglia, 2015), that has a larger extension and a regional character (Pelle et al., 2013a; Vingiani et al., 2014). The ash-bearing soil corresponds to the class VI weathering grade soil in the study area of the present work. Based on the rhyolitic composition of vesiculated micropumice fragments identified in this soil, its lateral continuity and constant pedostratigraphic position, the volcanic input can be related to late Pleistocene to Holocene eruptions of the Aeolian Islands archipelago spanning the last 42 ka (Pelle et al., 2013b; Vingiani et al., 2014). The most likely volcanic events are the explosive eruptions from Lipari that form the Valle Muria synthem (42-22 ka) (Crisci et al., 1991; Lucchi et al., 2013) and the Pollara eruptions (24-13 ka) from Salina (Keller, 1980; Calanchi et al., 1993). The corresponding volcanic deposits are dated on land in the archipelago and consistent with the tephrochronological records in proximal marine cores of the Tyrrhenian Sea (Paterne et al., 1988), and for the oldest eruptions as distal cryptotephra in the southern Adriatic Sea to the north-east (Matthews et al., 2015), in accordance with late Quaternary eastward dominant wind directions (Paterne et al., 1988). Their time constraints serve as a maximum age for the above cited

soil, which also postdates a paleosol of the last interglacial (Scarciglia et al., 2005b, 2008), includes charcoals whose older AMS radiocarbon date reaches 14 ka (Moser, unpublished data) and late Neolithic/early Eneolithic (ca. 5800-5350 a BP) to Roman (3^{rd} – 5^{th} century AD) archaeological settlements and artefacts (Pelle et al., 2013a, 2013b). Scarciglia (2015) demonstrated that the granodiorite spheroidal boulders exhumed at the topographic surface in the area around Silvana Mansio had been completely exposed by erosion before the volcanic input and the consequent formation of the soil. In fact, the latter covers the base of the exhumed boulders, whose lower exposed part is usually dirty and brown-colored as the soil itself, as a consequence of further recent exhumation. These boulders are classified as rocks of weathering grades I to I-II, and represent the deepest counterpart of an ideally 'complete' spheroidal weathering profile from fresh bedrock to saprock, up to saprolite and soil horizons (e.g., Migoń, 2013a, 2013b), later removed by erosive processes. On this basis, it is very likely that the weathering profiles nowadays observed beneath them, which include weathering grade classes from I-II to VI, developed after their exhumation. This feature allowed us to fix rough age constraints to assess the soil formation rates of these profiles. These rates were estimated for different (maximum) recurrent depths of the weathering profile zones, according to field data (see section 3.1), by dividing depth values by time: 50 and 100 cm for A and Bw horizons (class VI), respectively; 1.5 and 5 m for Cr or C layers (class V); 8 and 25 m, that represent the most common (maximum) depths of the exposed profiles (excluding intensely eroded soils and bare rock), reaching class (I-)II. Because of some age uncertainty of the soil discussed above, two endmember scenarios were considered as reference time ranges for the calculations, using (i) the potentially oldest volcanic input to the surface soil (42 ka) and (ii) the oldest ^{14}C date (14 ka). The obtained values of soil formation rates reported in Table 5 ranged from minima of 0.01 and 0.02 mm a^{-1} for A and Bw horizons, respectively, to 0.04-0.12 mm a^{-1} when including the underlying saprolite for the first scenario (42 ka). Weathering rates for deeper, less weathered rock layers were of 0.19 and 0.60 mm a^{-1}, respectively (42 ka). Higher rates were estimated for the 14 ka-constrained scenario, as follows: 0.04 mm a^{-1} (A horizon), 0.07 mm a^{-1} (Bw horizon), 0.11-0.36 mm a^{-1} (C or Cr layers), 0.57-1.79 mm a^{-1} (R layers). Nonetheless, the rates obtained for proper soil horizons exhibited the same order of magnitude for the two scenarios and shifted of one order for the saprolite and weathered bedrock.

4. Discussion

4.1 Weathering processes

4.1.1 Surface weathering versus inherited hydrothermal alteration

Both macro- and micromorphological discontinuities of the bedrock (including compositional changes) appear to have controlled modes and extent of physical and chemical weathering, acting as specific surface area prone to the onset of weathering processes and their dynamic progression (e.g., Ehlen, 2002; Anderson et al., 2007), with mutual down- and up-scaling effects (Viles, 2001, 2013). Tectonic activity and related structural features could be assumed to have a strong control on enhancement of physical breakdown and disintegration of rocks, as well as on the triggering of major chemical weathering processes. The multiscale joint systems associated to fault gouges, shear zones, thrust planes and any other fractures presumably acted as predisposing factors for preferential water flow and water-rock interaction, often leading to intense argillification (cf. Borrelli et al., 2012b, 2014, 2015a, 2015b). Similarly, at a microtextural level the chemical and crystallographic discontinuities (compositional zoning, cleavage and twinning planes) proved to control the location, modes and spatial patterns of the main weathering features affecting primary minerals, as preferential pathways for chemical reactions and physical breakage, with consequent rock decomposition (cf. Scarciglia et al., 2005a, 2007; von Eynatten et al., 2016). The observed chloritization of biotite is very likely derived from hydrothermal alteration of plutonic igneous masses of the Sila batholith during cooling (cf. Messina et al., 1991 and see below). The hydrothermal origin of chlorite is as also supported by its very low amount in the soil horizons overlying the granitoid parent materials of the study area, where it is easily transformed into vermiculite (Scarciglia et al., 2008; Apollaro et al., 2013a; Perri et al., 2015). The progressive exfoliation and oxidation of micas (especially biotite) from poorly to intensely weathered rock samples, coupled with an increasing clay neogenesis, were observed to generate a partial to complete flake separation along cleavage planes. This process in turn generates microcraks that propagate into surrounding, less weathered mineral grains, thus leading to a progressive biotite-induced grussification (Isherwood and Street, 1976; Scarciglia et al., 2007). The occurrence of iron-manganese segregations (and at a minor extent clay coatings) in the cracks radiating from weathered biotite grains already in classes II to III-IV indicates that circulating waters promote migration of these oxides (and neoformed clays) since early stages of weathering. A significant presence of Fe-Mn oxyhydroxide and clay infillings within cracks was detected in samples of weathering grade class V, where also clay- and iron-rich matrix zones appear as a late stage, in situ replacement of pseudomorphous mica grains. Our petrographic observations showed that plagioclase crystals are affected by a quite varying degree of chemical weathering, sometimes characterized by diffuse dissolution features and clay neogenesis even in classes II(-III) to III-IV, whereas K-feldspar appears poorly to moderately etched. This behavior suggests that in situ hydrolysis of plagioclase was enhanced by its pre-existing and often incomplete sericitization, that was presumably of deuteric

origin, i.e. developed in later stages of magma consolidation of the Sila pluton. The very common sericitization of the plagioclase generally limited to its core, along with the very rare and poor hydrothermal alteration of the alkali feldspar, suggest overall low fluid/rock ratios promoted by a limited access of hydrothermal fluids, possibly occurred during contractional cooling phases of the granite batholith (Que and Allen, 1996) rather than during later tectonic fracturing and dyke intrusion (Peters and Hofmann, 1984). Similarly, most of the biotite chloritization could be attributed to this stage of hydrothermal alteration (Peters and Hofmann, 1984). Late-stage fluid-rock interactions presumably occurred during the final phases of emplacement and slow cooling of the Sila batholith due to late-orogenic extension, with cooling of the exposed lower crustal rocks possibly terminated during the late Miocene (cf. Thomson, 1998; Graessner et al., 2000). This interpretation is supported by a late, mild hydrothermal alteration event identified in a few of the more evolved granitic rocks by De Vivo et al. (1991). The lack of evidence for intense and pervasive hydrothermal alteration in the Sila Massif (Ayuso et al., 1994), with an exception of the metasomatism created by fluid advection in the Longobucco area (Caggianelli et al., 2000; Perri et al., 2008), could be explained by the severe erosion documented in the study area, which might have removed large parts of the most altered rocks. Despite many weathering profiles clearly exhibit mesoscale tectonic features in the field (cf. section 2.1), a certain independence of part of the collected samples that include sericitized plagioclase and/or chloritized biotite from faults, major tectonic fissures and veins, supports that circulating fluids which led to hydrothermal alteration were not mainly related to the Pleistocene tectonics affecting the Sila Massif granitoids. A tectonic influence cannot be ruled out for a couple of sites close to important faults, especially in the Silvana Mansio area where alteration features are more pervasive (see section 3.2), and in the Longobucco surroundings where sericite is more abundant.

The neoformed clays identified on weathered primary minerals and in illuvial clay coatings consist of both 1:1 and 2:1 clays, such as kaolinite/halloysite, and illite, vermiculite and/or smectite components, in agreement with those reported for weathering profiles and soils in the Sila Massif (Scarciglia et al., 2008; Pelle et al., 2013b; Perri et al., 2015; Scarciglia, 2015). Coherently with increasing weathering grades, even quartz grains exhibited some chemical dissolution microtextures starting from classes III or IV. Despite the acidic pH measured in the soils of the study area (ARSSA, 2003; Scarciglia et al., 2005a, 2005b; Pelle et al., 2013b), quartz dissolution could have been controlled by alkali and alkaline-earth metals (Dove and Nix, 1997; Karlsson et al., 2001) at the microsite level, where a transient, locally alkaline soil environment could have been promoted by basic cations released from the weathering of primary feldspars and micas, possibly coupled with a long time of exposure to weathering processes (Scarciglia et al., 2007, 2015).

4.1.2 In situ weathering versus illuvial processes

The slight differences in composition between the measured samples of class I-II and those reported by Messina et al. (1991) virtually ascribed to class I(-II) (see section 3.3) can be easily related to intrinsic small compositional changes of the granitoid parent rocks, ranging from tonalite to monzogranite and granodiorite, and including different accessory phases. The chemical index of alterationrecords an incipient to intermediate chemical weathering stage (cf. Fedo et al., 1995). The overall decrease in SiO_2 as far as weathering grade increases (except in weathering class III-IV) is consistent with a progressive desilication from the most labile minerals, such as plagioclase, K-feldspar and micas (and more rarely from more resistant quartz). This is in turn associated to an increase of Al_2O_3, probably fixed in the neoformed phyllosilicate clays. Both the Al_2O_3/SiO_2 ratio and the CIA index support this interpretation. The apparent inconsistency of class III-IV and III samples with the above trends, respectively, suggests a partial downward mobilization and re-precipitation of aluminum and silica from overlying saprolite and/or soil layers (cf. White, 2005). This is in agreement with an increase in the amount of clay minerals in those classes, as evidenced by the identification of clay coatings/infillings of illuvial origin on rock surfaces/fractures. Also a similar anomalous behavior of other components (e.g., MnO, partly Fe_2O_3, Ni, etc.) suggests that their increase in intermediate weathering classes (III to IV) is not mainly due to in situ weathering, but rather to illuvial processes, as indicated by the iron-manganese coatings and mottles staining rock fractures in the field (and microcracks identified in thin sections). The initial decline of CaO followed by its less pronounced increase according to increasing weathering grades suggests its release from Ca-bearing minerals (mainly plagioclase) and leaching, followed by its fixation in or adsorption onto phyllosilicate clays such as smectite and vermiculite. A similar reversal in abundance is shown by Sr and Ba, which commonly replace calcium in Ca-minerals (Reimann et al., 2003). The opposite behavior of K_2O suggests its being trapped in neoformed clays (such as illite) after removal from primary K-feldspar and mica, and a further leaching from illite. This also applies to Rb^+, which preferentially replaces K^+ due to its similar ionic radius, and is thus enriched into clay minerals by weathering processes (cf. Wennrich et al., 2014). Adsorption onto reactive sites of soil organic matter may also affect elemental patterns, especially in A horizons (class VI), as suggested by Pb behavior. Lead may be in turn retained in clay minerals (Mongelli et al., 1998), as suggested by its pattern that is partially similar to that of alumina (Bauer and Velde, 2014). A more irregular pattern of Na_2O, MgO, Fe_2O_3, TiO_2 and some trace chemical species (e.g., vanadium, zinc and the lanthanides) can be interpreted as partly controlled by a complex interplay among weathering of dominant and accessory host minerals, leaching, incorporation into phyllosilicate clays and/or concentration by the above

quoted illuviation processes (cf. Laveuf and Cornu 2009; Scarciglia et al., 2011; Huang et al., 2015; Perri et al., 2015). The importance of adsorption mechanisms onto clays (and/or oxyhydroxides) and illuvial processes affecting the III-IV weathering grade samples is evidenced by higher peaks for this class of the ratios of Mg, K, Na, Fe, Si and Al oxides, as well as of mobile trace metals (e.g., Ba, Sr and V), versus titanium, which is usually considered as 'immobile'. This interpretation is supported by a similar behavior of the Rb/Sr (e.g., Wennrich et al., 2014) and Ba/Sr ratios, as Sr is selectively leached whereas Rb and Ba are enriched in secondary minerals (e.g., Wan et al., 2010), along with the Zr/Zn ratio, because in weathered settings Zn tends to be concentrated in the finest fractions (e.g., von Eynatten et al., 2016). Ce and La are fractionated and enriched relative to parent rocks during weathering (e.g., Mongelli, 1993; Mongelli et al., 1998), as suggested by their general trend of increase relative to Ti. The Ce/Ti and La/Ti ratios show higher values even in weathering grade class III-IV than classes IV and V. This behavior is consistent with the occurrence of the above cited illuvial processes involving both clay minerals and iron oxyhydroxides, where the lanthanides are commonly adsorbed (Laveuf and Cornu, 2009; Scarciglia et al., 2011). An analogous behavior between these REEs and TiO_2 suggests that although on the whole immobile, titanium tends to concentrate as a consequence of weathering processes in the fine fractions, where it is more stable just in the form of dioxide (Tyler, 2004; Scarciglia et al., 2015). The partly illuvial origin of clays/Fe-Mn oxyhydroxides in some low to intermediate weathering grade classes is additionally confirmed by some values of Ip higher than those obtained in moderately weathered classes. Indeed, the micropetrographic index does not take into account whether clay minerals and/or iron-oxides are produced in situ by direct weathering of primary mineral phases or are transported and deposited into rock cracks after downward migration (illuviation) through circulating water across the weathering/soil profile. In addition, inheritance of some grain microtextures from hydrothermal alteration of the parent rock can be misleading in evaluating a correct weathering degree in surface conditions (Stoops et al., 2010), as it may simulate a higher degree of weathering. The above quoted deuteric origin of both chloritized biotite and sericitized plagioclase crystals, rather than a result of surface (meteoric) weathering processes, could clearly cause an overestimation of weathered versus unweathered primary minerals in poorly weathered classes, thus leading to an average underestimation of Ip values of 0.1, up to a difference of 3.4 in the weathering class III-IV (data not shown). A very poor statistic correlation between Ip values and the sum of sericitized and chloritized grains corroborates the bias that affects the micropetrographic index in the estimation of the extent of weathering. However, the hydrothermal features may have acted as preferential predisposing factors for the onset of subsequent chemical weathering processes ('real' clay neogenesis and etching) under environmental conditions. The peculiar response of different rock samples to chemical weathering may be also caused by an intrinsic

variability of the mineralogical composition, such as in those samples where K-feldspar largely prevails over plagioclase. Alkali feldspar appears very rarely and at a very small extent affected by sericitization with respect to plagioclase, and less weathered as well. Some mineralogical (and thus geochemical) heterogeneity is also suggested by small changes in the Ti/Zr and Si/Zr ratios even in low weathering grade classes, because of the relatively immobile behavior of titanium, silica and zirconium. Of course, a differential sensitivity of primary minerals to chemical attack may clearly affect the comparability of weathered/unweathered components quantification in different samples, definitely influencing the reliability of the micropetrographic index.

4.1.3 Chemical versus physical weathering

The apparent discrepancy detected between physical-mechanical field tests of rock strength with the geological and/or Schmidt hammer clearly suggests that chemical weathering of granitoid substrata is not always coupled with its physical degradation. This behavior can be explained by a significant role played by physical breakage processes in addition to dissolution, hydrolysis and reduction/oxidation. Cryoclastic and thermoclastic processes, that are well-documented at present in the study area (Scarciglia et al., 2005a, 2005b), presumably actively contribute to rock degradation and fragmentation in addition to the predisposing role of tectonics discussed above. Some authors (e.g., Butzer, 1976; Migoń and Thomas, 2002) suggest that cryogenic processes related to freeze-thaw cycles could be responsible for important grussification, as supported by the dominant coarse texture of weathered layers and soil horizons. Paleoclimatic reconstructions (Dimase, 2006) suggest that these processes could have been particularly intense during Pleistocene glacial phases in the Sila mountains, leading to friable or disintegrated debris (Scarciglia et al., 2007). The abundance of coarse-textured rock material in all parts of the studied weathering profiles, coupled with the various evidence of illuvial processes including important iron-oxide and clay translocation, suggests that more clay-enriched saprolite layers and soil horizons, argillified after hydrolysis of primary phases, formed in the past over the lower weathering grade rock classes. Hence the present-day profiles are clearly truncated and rejuvenated by long-term erosion, similarly to the boulders exposed at the ground floor (Scarciglia, 2015).

4.2 Soil formation rates

The contribution of volcanic ash to soil formation in the study area is very difficult to estimate, because it is at present very poor in the soil and pedogenesis occurred at the expenses of both the pumice and the granitoid parent materials, with consequent transformation into clay minerals (cf.

Scarciglia et al., 2008; Pelle et al., 2013b). The distal depositional environment in respect of the volcanic source area (Aeolian Islands), the occurrence as rare, micron-sized glass fragments dispersed in the pedogenic matrix and as distal cryptotephra in a north-eastern marine core, the granitic nature of skeletal rock fragments (Scarciglia et al., 2005a, 2005b) and the weakly andic properties of the soil (Scarciglia et al., 2008; Vingiani et al., 2014) suggest an important contribution of the granite parent material to soil formation. However, the more labile volcanic glass than the crystalline (alumino-)silicate primary components can be supposed to have promoted faster soil formation rates than in pure granitoid terrains. This does not attain directly to the saprolite and bedrock, where no volcanic components were detected, but clay formation and illuviation from the upper ash-bearing soil horizons could have affected indirectly even C, Cr and/or R layers. The soil formation rates estimated in this work for the Sila upland, especially those related to the 42 ka-constrained scenario, are consistent with a large number of data available in the literature, obtained with varying methods (uranium-series isotope disequilibria, cosmogenic radionuclide inventories, geochemical mass-balance modeling and residence time approach) for several areas with different geographic position but overall similar bedrock and climatic conditions (e.g., Heimsath et al., 2001; Riebe et al., 2001; Dosseto et al., 2008; Dixon et al., 2009; Suresh et al., 2013). These literature weathering and soil production rates mainly range from ≤ 0.01 to 0.14 mm a^{-1} and overlap all our estimates on saprolite and soil horizons (classes V-VI) for the 42 ka scenario, and partly for the 14 ka scenario. The chronological constraints which permitted to obtain these rates (see section 3.4) are consistent with the expected time ranges of specific weathering and soil-forming processes, such as clay neogenesis (10^2-10^4 a), redox processes leading to different types of Fe- and Mn-oxide segregations (10^2-10^6 a), organic matter accumulation and storage (10^1-10^3 a) (e.g., Harden, 1987; Baisden et al., 2002; Targulian and Krasilnikov, 2007; Cornu et al., 2009). The weathering rates calculated for the deepest weathering profile zones underlying the proper saprolite layers and soil horizons, classified with lower weathering grades (I-II to IV), seem to be much less reliable. In fact, these weathering zones still maintain part of the original rock structure and fabric, and are often characterized by large amounts of illuvial features, that clearly refer to non-in-situ weathering.

Our results feed and renew the ongoing scientific debate on some presumably ‘old’ weathering mantles, such as some sandy saprolites (or ‘grus weathering profiles’) in Europe, that proved to be quite young, pointing to Quaternary rather than to Tertiary weathering (e.g., Migoń, 1997). This issue is consistent with intrinsic methodological flaws, such as the possible shielding effect of ice caps affecting ^{10}Be method applied in formerly glaciated areas (Migoń and Lidmar-Bergström, 2002), or the truncation of weathering profiles clearly evidenced in this paper, possibly caused by severe erosion phases since the middle Pleistocene (Scarciglia, 2015), in turn enhanced by high tectonic

uplift rates (Molin et al., 2012; Olivetti et. al., 2012). Geomorphological/pedological-based erosion rates (<0.01-0.05 to 0.10-0.21 mm a^{-1}; Scarciglia, 2015), preliminary cosmogenic ^{10}Be data from the basal portion of spheroidal boulders in the Silvana Mansio area (0.001-0.10 mm a^{-1}; Scarciglia and Egli, unpublished data), as well as ^{10}Be erosion rates from river systems (ca. 0.09-0.13 mm a^{-1}; Olivetti et. al., 2012) estimated for the Sila Massif upland, are consistent with uplift-driven Pleistocene erosion rates estimated in various areas of the southern Apennines (north of the Calabria region), which range between 0.04 and 0.6 mm a^{-1} (Amato et al., 2003; Schiattarella et al., 2006; Martino et al., 2009; Gioia et al., 2011). The highest values obtained for the Apennine Chain were likely promoted by lithologies on the whole less resistant to erosion than the Sila granitoids, whose summit paleolandscape appears less fragmented by tectonic faulting and headward-migrating (retrogressive) fluvial dissection (Martino et al., 2009; Schiattarella et al., 2013). Olivetti et. al. (2012) calculated even higher ^{10}Be erosion rates in the deeply incised river valleys along the Sila Massif flanks, reaching up to about 1 mm a^{-1}, whereas for the Aspromonte Massif (another tectonically active area in southern Calabria with similar relief features and evolution), Cyr et al. (2014) estimated rates between 0.6 and 2.1 mm a^{-1}. Also Ibbeken and Schleyer (1991), using missing volume and mass balance approaches, estimated long-term (1 Ma) erosion rates of 0.2 mm a^{-1}, with higher short-term rates of 0.9-1.9 mm a^{-1} up to a maximum of 2.7 mm a^{-1} in the fluvial systems. Although fluvial erosion rates can be expected to be higher than land surface erosion rates (where the action of concentrated water flow is less effective), there is a coherence between the soil formation rates obtained on the summit flat landforms of the study area and the erosion rates associated to sediment delivery into the drainage system. Overall comparable values of soil formation and long-term erosion rates in the summit landscape suggest conditions close to a dynamic equilibrium (steady state) between the deepening of the weathering front (soil production, i.e. bedrock conversion to weathered products) and the removal of the regolith by morphodynamic processes (erosion) (Riebe et al., 2003; Anderson et al., 2007; Heimsath et al., 2012). Such an equilibrium is not necessarily strictly achieved, as changes in sediment generation rates over time (possibly driven by climatic and/or tectonic forcing) can be buffered by the soil mantle, where potentially erodible materials may be stored for millennia before entering the river system (Bierman and Nichols, 2004). Where soils mantle hillslopes, soil formation (and sediment production) rates exceed transport capacity, whereas where bare rock slopes dominate, sediment transport rates exceed those of regolith production. Higher erosion rates in the fluvial system, which can be considered as basin-scale average rates of erosion equivalent to rates of sediment generation (Bierman and Nichols, 2004; Heimsath et al., 2012), indicate that these are not in balance with sediment yields.

5. Conclusions

An integrated analysis of large datasets, including novel and partly published morphological, geomechanical, petrographic, mineralogical and geochemical features of weathered granitoid rocks in a wide area of the Sila Massif upland (Calabria, southern Italy), allowed us a deeper comprehension of the weathering profile patterns and corresponding weathering processes. First of all, we remarked the potentially misleading effects of hydrothermal alteration of some primary minerals (such as sericitization of plagioclase and chloritization of biotite) on the evaluation of a correct degree of weathering. These inherited features may induce an overestimation of effective meteoric weathering, although they may also control and enhance chemical dissolution and clay neogenesis in surface conditions. Secondly, our results showed that a mere field description of weathering profiles or a simple identification of weathering products may not take into account the in-situ versus illuvial genesis of some morphological features (at the macro- and microscales). Actually, changes in color of the weathered materials in respect to the parent rock were observed to originate in places by local neogenesis of phyllosilicate clays or release of iron and manganese in the form of oxyhydroxides on mineral grain surfaces (especially biotite or chlorite crystals), whereas in other places they appeared to be illuviated as coatings into rock cracks and thus not formed in situ. These features produced some apparent inconsistencies between the classification of weathering grades based on field observations coupled with geomechanical tests and the chemical index of alteration (CIA) or the micropetrographic index (Ip). In addition to the effects of illuvial processes, some discrepancies between the results from the above methodological approaches were explained as caused by other weathering processes than chemical weathering. Cryoclastic and thermoclastic processes promote a physical breakdown besides tectonics even in rock masses that are relatively poorly affected by chemical weathering features. Our results showed that particular caution is required for a correct assessment of weathering grade classes, because inherited hydrothermal alteration features, physical weathering and illuvial processes may affect results obtained from traditional field and geochemical-petrographic tools.

Finally, a first estimation of soil formation rates was proposed in this paper for different depths of weathering profile zones, based on radiocarbon and tephrochronological constraints. The obtained values ranged from 0.01-0.07 mm a^{-1} for A and Bw horizons (weathering grade class VI) to 0.04-0.36 mm a^{-1} for the underlying saprolitic layers C and Cr (class V). These results are consistent with worldwide literature data for areas with similar bedrock and climate, and are on the whole comparable to the erosion rates estimated for the same site and other areas of southern Italy. This behavior suggests that the upland landscape of the Sila Massif is close to steady-state conditions between weathering and erosive processes.

Acknowledgments

Support from Ministero dell'Istruzione, dell'Università e della Ricerca (MIUR), Università della Calabria (ex-60% Projects; grants to S. Critelli and F. Scarciglia), and Laboratory of Geodynamics, Paleo-Geobiology and Earth Surface Processes are acknowledged. We are grateful to Deborah Biondino, Maria Maddalena Piane and Cesare Zumpano for some laboratory analyses. We are indebted to two anonymous reviewers for their constructive comments that greatly helped to improve our manuscript.

References

Amato, A., Aucelli, P.P.C., Cinque, A., 2003. The long-term denudation rate in the Southern Apennines Chain (Italy): a GIS-aided estimation of the rock volumes eroded since middle Pleistocene time. Quaternary International 101–102, 3–11.

Apollaro, C., Accornero, M., Marini, L., Barca, D., De Rosa, R., 2009. The impact of dolomite and plagioclase weathering on the chemistry of shallow groundwaters circulating in a granodiorite-dominated catchment of the Sila Massif (Calabria, Southern Italy). Applied Geochemistry 24, 957–979.

Apollaro, C., Marini, L., Critelli, T., De Rosa, R., 2013a. The standard thermodynamic properties of vermiculites and prediction of their occurrence during water–rock interaction. Applied Geochemistry 35, 264–278.

Apollaro, C., Marini, L., Critelli, T., De Rosa, R., Bloise, A., Miriello, D., Catalano, M., Armano, V., 2013b. Modeling of the impact of dolomite and biotite dissolution on vermiculite composition in a gneissic shallow aquifer of the Sila Massif (Calabria, Italy). Applied Geochemistry 35, 297–311.

Anderson, S.P., von Blanckenburg, F., White, A.F., 2007. Physical and chemical controls on the Critical Zone. Elements 3 (5), 315–319.

Arel, E., Tugrul, A., 2001. Weathering and its relation to geomechanical properties of Cavusbasi granitic rocks in northwestern Turkey. Bulletin of Engineering Geology and the Environment 60, 123–133.

Arikan, F., Aydin, N., 2012. Influence of weathering on the engineering properties of dacites in northeastern Turkey. ISRN (International Scholarly Research Network) Soil Science 2012, Article ID 218527, 1–15.

Arribas, J., Critelli, S., Le Pera, E., Tortosa, A., 2000. Composition of modern stream sand derived from a mixture of sedimentary and metamorphic rocks (Henares River, central Spain). Sedimentary Geology 133, 27–48.

ARSSA (Agenzia Regionale per lo Sviluppo e per i Servizi in Agricoltura), 2003. I suoli della Calabria. Carta dei suoli in scala 1:250000 della Regione Calabria. Monografia divulgativa. Programma Interregionale Agricoltura-Qualità –Misura 5, ARSSA, Servizio Agropedologia. Rubbettino, Italy, 387 pp.

Ayuso, R.A., Messina, A., De Vivo, B., Russo, S., Woodruff, L.G., Sutter, J.F., Belkin, H.E., 1994. Geochemistry and argon thermochronology of the Variscan Sila Batholith, southern Italy: source rocks and magma evolution. Contributions to Mineralogy and Petrology, 117, 87–109.

Baisden, W.T., Amundson, R.G., Brenner, D.L., Cook, A.C., Kendall, C., Harden, J.W., 2002. A multi-isotope C and N modeling analysis of soil organic matter turnover and transport as a function of soil depth in a California annual grassland soil chronosequence. Global Biogeochemical Cycles 16 (4), 1135, 1–26.

Barone, M., Dominici, R., Muto, F., Critelli, S., 2008. Detrital modes in a late Miocene wedge-top basin, northeastern Calabria, Italy: compositional record of wedge-top partitioning. Journal of Sedimentary Research 78, 693–711.

Bauer, A., Velde, B.D., 2014. Weathering: the initial transition to surface material and the beginning of surface geochemistry. Chapt. 3, Geochemistry at the Earth's surface. Movement of chemical elements. Springer-Verlag, Berlin Heidelberg, pp. 101–156.

Bierman, P.R., Nichols, K.K., 2004. Rock to sediment – slope to sea with ^{10}Be – rates of landscape change. Annual Review of Earth and Planetary Sciences 32, 215–255.

Birkeland, P.W., 1999. Soils and Geomorphology. Oxford University Press, New York, 430 pp.

Blum, J.D., Erel, Y., 1997. Rb–Sr isotope systematics of a granitic soil chronosequence: the importance of biotite weathering. Geochimica et Cosmochimica Acta 15, 3193–3204.

Bonardi, G., Cavazza, W., Perrone, V., Rossi, S., 2001. Calabria-Peloritani Terrane and northern Ionian Sea. In: Vai, G.B., Martini, J.P. (Eds.), Anatomy of an orogen: The Apennines and the adjacent Mediterranean basins. Kluwer Academic, Norwell, MA, pp. 287–306.

Borrelli, L., Greco, R., Gullà, G., 2007. Weathering grade of rock masses as a predisposing factor to slope instabilities: reconnaissance and control procedures. Geomorphology, 87, 158–175.

Borrelli, L., Cofone, G., Gullà, G., 2012a. Procedura speditiva per la redazione di una carta del grado di alterazione a scala regionale. Rendiconti Online della Società Geologica Italiana 21, 528–530.

Borrelli, L., Perri, F., Critelli, S., Gullà, G., 2012b. Minero-petrographical features of weathering profiles in Calabria, southern Italy. Catena 92, 196–207.

Borrelli, L., Cofone, G., Critelli, S., Greco, S., Gullà, G., 2012c. Carta del grado di alterazione e categorie di frane nell'alta valle del Fiume Trionto (Calabria, Italia). Rendiconti Online della Società Geologica Italiana, 21, 537–539.

Borrelli, L., Perri, F., Critelli, S., Gullà, G., 2014. Characterization of granitoid and gneissic weathering profiles of the Mucone River basin (Calabria, southern Italy). Catena 113, 325–340.

Borrelli, L., Coniglio, S., Critelli, S., La Barbera, A., Gullà, G., 2015a. Weathering grade in granitoid rocks: The San Giovanni in Fiore area (Calabria, Italy). Journal of Maps, 1-16, doi: 10.1080/17445647.2015.1010742

Borrelli, L., Critelli, S., Gullà, G., Muto, F., 2015b. Weathering grade and geotectonics of the western-central Mucone River basin (Calabria, Italy). Journal of Maps 11 (4), 606–624, doi: 10.1080/17445647.2014.933719

Bourke, M., Viles, H. (Eds.), 2007. A Photographic Atlas of Rock Breakdown Features in Geomorphic Environments. Planetary Science Institute, Tucson, Arizona, USA, 79 pp.

Buss, H.L., Sak, P.B., Webb, S.M., Brantley, S.L., 2008. Weathering of the Rio Blanco quartz diorite, Luquillo Mountains, Puerto Rico: Coupling oxidation, dissolution, and fracturing. Geochimica et Cosmochimica Acta 72, 4488–4507.

Butzer, K.W., 1976. Geomorphology from the Earth. Harper and Row Publishers, New York, 463 pp.

Caggianelli, A., Prosser, G., Rottura, A., 2000. Thermal history vs. fabric anisotropy, in granitoids emplaced at different crustal levels: an example from Calabria, southern Italy. Terra Nova 12 (3), 10–116.

Calanchi, N., De Rosa, R., Mazzuoli, R., Rossi, P.L., Santacroce, R., Ventura, G., 1993. Silicic magma entering a basaltic magma chamber: eruptive dynamics and magma mixing d an example from Salina (Aeolian islands, Southern Tyrrhenian Sea). Bulletin of Volcanology 55, 504–522.

Campodonico, V.A., Martínez, J.O., Verdecchia, S.O., Pasquini, A.I., Depetris, P.J., 2014. Weathering assessment in the Achala Batholith of the Sierra de Comechingones, Córdoba, central Argentina. I: Granite–regolith fractionation. Catena 123, 121–134.

Caracciolo, L., Tolosana-Delgado, R., Le Pera, E., von Eynatten, H., Arribas, J., Tarquini, S., 2012. Influence of granitoid textural parameters on sediment composition: Implications for sediment generation. Sedimentary Geology 280, 93–107.

Chabaux, F., Blaes, E., Stille, P., di Chiara Roupert, R., Pelt, E., Dosseto, A., Ma, L., Buss, H.L., Brantley, S.L., 2013. Regolith formation rate from U-series nuclides: Implications from the study of a spheroidal weathering profile in the Rio Icacos watershed (Puerto Rico). Geochimica et Cosmochimica Acta 100, 73–95.

Chigira, M., Yokoyama, O., 2005. Weathering profile of non-welded ignimbrite and the water infiltration behavior within it in relation to the generation of shallow landslides. Engineering Geology 78, 187–207.

Chiu, C.F., Ng, C.W.W., 2014. Relationships between chemical weathering indices and physical and mechanical properties of decomposed granite. Engineering Geology 179, 76–89.

Corbi, F., Fubelli, G., Lucà, F., Muto, F., Pelle, T., Robustelli, G., Scarciglia, F., Dramis, F., 2009. Vertical movements in the Ionian margin of the Sila Massif (Calabria, Italy). Bollettino della Società Geologica Italiana 128, 731–738.

Cornu, S., Montagne, D., Vasconcelos, P.M., 2009. Dating constituent formation in soils to determine rates of soil processes: A review. Geoderma 153, 293–303.

Crisci, G.M., De Rosa, R., Esperanca, S., Mazzuoli, R., Sonnino, M., 1991. Temporal evolution of a three component system: the Island of Lipari (Aeolian Arc, southern Italy). Bulletin of Volcanology 53, 207–221.

Critelli, S., 1993. Sandstone detrital modes in the Paleogene Liguride Complex, accretionary wedge of the Southern Apennines (Italy). Journal of Sedimentary Petrology 63, 464–476.

Critelli, S., Le Pera, E., 1995. Tectonic evolution of the Southern Apennines thrust-belt (Italy) as reflected in modal compositions of Cenozoic sandstone. Journal of Geology 103, 95–105.

Critelli, S., Le Pera, E., 1998. Post-Oligocene sediment dispersal systems and unroofing history of the Calabrian Microplate, Italy. International Geology Review, 48, 609–637.

Critelli, S., Le Pera, E., 2002. Provenance relations and modern sand petrofacies in an uplifted thrust-belt, northern Calabria, Italy. Memorie Descrittive della Carta Geologica d'Italia 51, 25–38.

Critelli, S., Di Nocera, S., Le Pera, E., 1991. Approccio metodologico per la valutazione petrografica del grado di alterazione degli gneiss del Massiccio Silano (Calabria settentrionale). Geologia Applicata e Idrogeologia 26, 41–70.

Critelli, S., Arribas, J., Le Pera, E., Tortosa, A., Marsaglia, K.M., Latter, K.K., 2003. The recycled orogenic sand provenance from an uplifted thrust-belt, Betic Cordillera, southern Spain. Journal of Sedimentary Research 73, 72–81.

Critelli, S., Muto, F., Tripodi, V., Perri, F., 2011. Relationships between lithospheric flexure, thrust tectonics and stratigraphic sequences in foreland setting: the southern Apennines foreland basin system, Italy. In: Schattner U (ed) New frontiers in tectonic research – at the midst of plate convergence. InTech, Rijeka, pp. 121–170.

Critelli, S., Muto, F., Tripodi, V., Perri, F., 2013. Link between thrust tectonics and sedimentation processes of stratigraphic sequences from the southern Apennines foreland basin system, Italy. Rendiconti Online della Società Geologica Italiana 25, 21–42.

Cyr, A.J., Granger, D.E., Olivetti, V., Molin, P., 2014. Distinguishing between tectonic and lithologic controls on bedrock channel longitudinal profiles using cosmogenic ^{10}Be erosion rates and channel steepness index. Geomorphology 209, 27–38.

Darmody, R.G., Thorn, C.E., Allen, C.E., 2005. Chemical weathering and boulder mantles, Kärkevagge, Swedish Lapland. Geomorphology 67, 159–170.

De Vivo, B., Ayuso, R.A., Belkin, H.E., Lima, A., Messina, A., Viscardi, A., 1991. Rock chemistry and fluid inclusion studies as exploration tools for ore deposits in the Sila Batholith, southern Italy. Journal of Geochemical Exploration 40, 291–310.

Dimase, A.C., 2006. Fossil cryogenic features in paleosols of southern Italy: Characteristics and paleoclimatic significance. Quaternary International 156–157, 32–48.

Dimase, A.C., Iovino, F., 1996, I suoli dei bacini idrografici del Trionto, Nicà e torrenti limitrofi (Calabria), with 1:100,000 scale map. Pubblicazioni dell'Accademia Italiana di Scienze Forestali, Nuova Stamperia Parenti, Firenze, Italy,112 pp.

Dixon, J.C., 2013. Chemical weathering in cold climates. In: Shroder, J.F. (Ed.), Treatise on geomorphology, vol. 4, chapter 14 – Weathering and soils geomorphology. Academic, Press, San Diego, pp. 245–257.

Dixon, J.C., Thorn, C.E., 2005. Chemical weathering and landscape development in mid-latitude alpine environments. Geomorphology 67, 127–145.

Dixon, J.L., Heimsath, A.M., Amundson, R., 2009. The critical role of climate and saprolite watheirng in landscape evolution. Earth Surface Processes and Landforms 34, 1507–1521.

Dosseto, A., Turner, S.P., Chappell, J., 2008. The evolution of weathering profiles through time: new insights from uranium-series isotopes. Earth and Planetary Science Letters 274, 359–371.

Dove, P.M., Nix, C.J., 1997. The influence of alkaline earth cations, magnesium, calcium and barium on the dissolution kinetics of quartz. Geochimica et Cosmochimica Acta 61 (16), 3329–3340.

Egli, M., Dahms, D., Norton, K., 2014. Soil formation rates on silicate parent material in alpine environments: Different approaches–different results? Geoderma 213, 320–333.

Ehlen, J., 2002. Some effects of weathering on joints in granitic rocks. Catena 49, 91–109.

Fabbricatore, D., Robustelli, G., Muto, F., 2014. Facies analysis and depositional architecture of shelf-type deltas in the Crati Basin (Calabrian Arc, south Italy). Italian Journal of Geosciences 133, 131–148.

Fedo, C.M., Nesbitt, H.V., Young, G.M., 1995. Unraveling the effects of potassium metasomatism in sedimentary rocks and paleosols, with implications for paleoweathering conditions and provenance. Geology 23, 921–924.

Geotechnical Engineering Office (GEO), 1988. Guide to rock and soil descriptions. Civil Engineering Department, The Government of the Hong Kong Special Administrative Region, Hong Kong, pp. 186.

Gioia, D., Martino, C., Schiattarella, M., 2011. Long- to short-term denudation rates in the southern Apennines: geomorphological markers and chronological constraints. Geologica Carpathica 62 (1), 27–41.

Gong, Q., Deng, J., Yang, L., Zhang, J., Wang, Q., Zhang, G., 2011. Behavior of major and trace elements during weathering of sericite–quartz schist. Journal of Asian Earth Sciences 42, 1–13.

Graessner, T., Schenk, V., Bröcker, M., Mezger, K., 2000. Geochronological constraints on the timing of granitoid magmatism, metamorphism and post-metamorphic cooling in the Hercynian crustal cross-section of Calabria. Journal of Metamorphic Geology 18, 409–421.

Gullà, G., Matano, F., 1997. Surveys of weathering profile on gneiss cutslopes in northern Calabria, Italy. Proceedings of the International Symposium on Engineering Geology and the Environment, IAEG, Athens, Greece, 23-27 June 1997, pp. 133–138.

Harden, J.W., 1987. Soils developed on granitic alluvium near Merced, USGS, California. U.S. Geological Survey Bulletin 1590-A, A1–A65.

Harnois, 1988. The CIW Index: a new chemical index for weathering. Sedimentary Geology 55, 319–322.

Haskins, D., 2006. Chemical and mineralogical weathering indices as applied to a granite saprolite in South Africa. Proceedings of the 10th Congress of the International Association for Engineering Geology and the Environment, Nottingham, United Kingdom, 6-10 September 2006, IAEG 2006 Paper number 465, pp. 1–14.

Heidari, M., Momeni, A.A., Naseri, F., 2013. New weathering classifications for granitic rocks based on geomechanical parameters. Engineering Geology 166, 65–73.

Heimsath, A.M., DiBiase, R.A., Whipple, K.X., 2012. Soil production limits and the transition to bedrock-dominated landscapes. Nature Geoscience 5, 210–214.

Heimsath, A.M., 2006. Eroding the land: steady-state and stochastic rates and processes through a cosmogenic lens. In: Siame, L.L., Bourlès, D.L., Brown, E.T. (Eds.), In situ–produced cosmogenic nuclides and quantification of geological processes. Geological Society of America Special Paper 415, pp. 111–129.

Heimsath, A.M., Chappell, J., Dietrich, W.E., Nishiizumi, K., Finkel, R.C., 2001. Late Quaternary erosion in southeastern Australia: a field example using cosmogenic nuclides. Quaternary International 83–85,169–185.

Huang, L., Liu, F., Tan, W.-F., Wang, M.-K., 2015. Geochemical characteristics of trace elements in argillans of Alfisols in central China. Pedosphere 25 (3), 415–427.

Ibbeken, H., Schleyer, R., 1991. Source and sediment. A case study of provenance and mass balance at an active plate margin (Calabria, southern Italy). Springer, Berlin, 286 pp.

Irfan, T.Y., Dearman, W.R., 1978. The engineering petrography of a weathered granite in Cornwall, England. Quarterly Journal of Engineering Geology 11, 223–244.

Isherwood, D., Street, A., 1976. Biotite-induced grussification of Boulder Creek Granodiorite, Boulder County, Colorado. Geological Society of America Bulletin 87, 366–370.

Johnsson, M.J., 1993. The system controlling the composition of clastic sediments. In: Johnsson, M.J., Basu A. (Eds.), Processes controlling the composition of clastic sediments. Geological Society of America Special Paper 284, pp. 1–19.

Karlsson, M., Craven, C., Dove, P.M., Casey, W.H., 2001. Surface charge concentrations on silica in different 1.0 M metal-chloride background electrolytes and implications for dissolution rates. Aquatic Geochemistry 7, 13–32.

Keller, J., 1980. The Island of Salina. Rendiconti della Società Italiana di Mineralogia e Petrologia 36, 489–524.

Kirschbaum, A., Martínez, E., Pettinari, G., Herrero, S., 2005. Weathering profiles in granites, Sierra Norte (Co´rdoba, Argentina). Journal of South American Earth Sciences 19, 479–493.

Kretzschmar, R., Robarge, W.P., Amoozegar, A., Vepraskas, M.J., 1997. Biotite alteration to halloysite and kaolinite in soil-saprolite profiles developed from mica schist and granite gneiss. Geoderma 75, 55–170.

Laveuf, C., Cornu, S., 2009. A review on the potentiality of Rare Earth Elements to trace pedogenetic processes. Geoderma 154, 1–12.

Le Pera, E., Arribas, J., 2003. san composition in an Iberian passive-margin fluvial course: the Tajo River. Sedimentary Geology 171, 261–281.

Le Pera, E., Sorriso-Valvo, M., 2000a. Weathering and morphogenesis in a Mediterranean climate, Calabria, Italy. Geomorphology 34, 251–270.

Le Pera, E., Sorriso-Valvo, M., 2000b. Weathering, erosion and sediment composition in a high-gradient river, Calabria, Italy. Earth Surface Processes and Landforms 25, 277–292.

Le Pera, E., Arribas, J., Critelli, S., Tortosa, A., 2001a. The effects of source rocks and chemical weathering on the petrogenesis of siliciclastic sand from the Neto River (Calabria, Italy): implications for provenance studies. Sedimentology 48, 357–378.

Le Pera, E., Critelli, S., Sorriso-Valvo, M., 2001b. Weathering of gneiss in Calabria, Southern Italy. Catena 42, 1–15.

Liotta, D., Caggianelli, A., Kruhl, J.H., Festa, V., Prosser, G., Langone, A., 2008. Multiple injections of magmas along a Hercynian mid-crustal shear zone (Sila Massif, Calabria, Italy). Journal of Structural Geology 30, 1202–1217.

Lucchi, F., Tranne, C.A., Forni, F., Rossi, P.L., 2013. Geological map of the island of Lipari, scale 1:10000 (Aeolian Archipelago). In: Lucchi, F., Peccerillo, A., Keller, J., Tranne, C.A., Rossi, P.L. (Eds.), The Aeolian Islands Volcanoes. Geological Society, London, Memoirs 37, Enclosed Dvd.

Lumb, P., 1962. The properties of decomposed granite. Geotecnique 12, 226–243.

Martino, C., Nico, G., Schiattarella, M., 2009. Quantitative analysis of InSAR Digital Elevation Models for identification of areas with different tectonic activity in southern Italy. Earth Surface Processes and Landforms 34, 3–15.

Matano, F., Di Nocera, S., 1999. Weathering patterns in the Sila Massif (Northern Calabria, Italy). Il Quaternario – Italian Journal of Quaternary Sciences 12 (2), 141–148.

Matthews, I.P., Trincardi, F., Lowe, J.J., Bourne, A.J., MacLeod, A., Abbott, P.M., Andersen, N., Asioli, A., Blockley, S.P.E., Lane, C.S., Oh, Y.A., Satow, C.S., Staff, R.A., Wulf, S., 2015. Developing a robust tephrochronological framework for Late Quaternary marine records in the Southern Adriatic Sea: new data from core station SA03-11. Quaternary Science Reviews 118, 84–104.

Mavris, C., Götze, J., Plötze, M., Egli, M., 2012. Weathering and mineralogical evolution in a high Alpine soil chronosequence: A combined approach using SEM–EDX, cathodoluminescence and Nomarski DIC microscopy. Sedimentary Geology 280, 108–118.

Messina, A., Barbieri, M., Compagnoni, R., De Vivo, B., Perrone, V., Russo, S., Scott, B.A., 1991. Geological and petrochemical study of the Sila Massif plutonic rocks (northern Calabria, Italy). Bollettino della Società Geologica Italiana 110, 165–206.

Messina, A., Somma, R., Macaione, E., Carbone, G., Careri, G., 2004. Peloritani continental crust composition (southern Italy): geological and petrochemical evidence. Bollettino della Società Geologica Italiana 123, 405–441.

Migoń, P., 1997. Palaeoenvironmental significance of grus weathering profiles: a review with special reference to northern and central Europe. Proceedings of the Geologists' Association, 108, 57–70.

Migoń, P., 2013a. Weathering and hillslope development. In: Shroder, J.F. (Ed.), Treatise on geomorphology, vol. 4, chapter 10 – Weathering and soils geomorphology. Academic Press, San Diego, pp. 159–178.

Migoń, P., 2013b. Weathering mantles and long-term landform evolution. In: Shroder, J.F. (Ed.), Treatise on geomorphology, vol. 4, chapter 8 – Weathering and soils geomorphology. Academic, Press, San Diego, pp. 127–144.

Migoń, P., Lidmar-Bergström, K., 2002. Deep weathering through time in central and NW Europe: problems of dating and interpretation of geological record. Catena 49 (1), 25–40.

Migoń, P., Thomas, M.F., 2002. Grus weathering mantles — problems of interpretation. Catena 49 (1), 5–24.

Migoń, P., Vieira, G., 2014. Granite geomorphology and its geological controls, Serra da Estrela, Portugal. Geomorphology 226, 1–14.

Molin, P., Pazzaglia, F.J., Dramis, F., 2004. Geomorphic expression of active tectonics in a rapidly-deforming forearc, Sila Massif, Calabria, southern Italy. American Journal of Science 304, 559–589.

Molin, P., Fubelli, G., Dramis, F., 2012. Evidence of tectonic influence on drainage evolution in an uplifting area: the case of northern Sila (Calabria, Italy). Geografia Fisica e Dinamica Quaternaria 35, 49–60.

Mongelli, G., 1993. REE and other trace elements in a granitic weathering profile from "Serre", southern Italy. Chemical Geology 103, 17–25.

Mongelli, G., Cullers, R.L., Dinelli, E., Rottura, A., 1998. Elemental mobility during the weathering of exposed lower crust: the kinzigitic paragneisses from the Serre, Calabria, southern Italy. Terra Nova 10, 190–195.

Mulyanto, B., Stoops, G., Van Ranst, E., 1999. Precipitation and dissolution of gibbsite during weathering of andesitic boulders in humid tropical West Java, Indonesia. Geoderma 89, 287–305.

Muto, F., Spina, V., Tripodi, V., Critelli, S., Roda, C., 2014. Neogene tectonostratigraphic evolution of allochthonous terranes in the eastern Calabrian foreland (southern Italy). Italian Journal of Geosciences 133 (3), 455–473.

Nesbitt, H.V., Fedo, C.M., Young, G.M., 1997. Quartz and feldspar stability, steady and non-steady-state weathering, and petrogenesis of siliciclastic sands and muds. Journal of Geology 105, 173–191.

Nesbitt, H.V., Young, G.M., 1982. Early Proterozoic climates and plate motions inferred from major element chemistry of lutites. Nature 299, 715–717.

Olivetti, V., Cyr, A.J., Molin, P., Faccenna, C., Granger, D.E., 2012. Uplift history of the Sila Massif, southern Italy, deciphered from cosmogenic ^{10}Be erosion rates and river longitudinal profile analysis. Tectonics 31, TC3007, 1–19.

Palomares, M., Arribas, J., 1993. Modern stream sands from compound crystalline sources: composition and sand generation index. In: Johnsson, M.J., Basu A. (Eds.), Processes controlling the composition of clastic sediments. Geological Society of America Special Paper 284, pp. 313–322.

Paterne, M., Guichard, F., Labeyrie, J., 1988. Explosive activity of the South Italian volcanoes during the past 80,000 years as determined by marine tephrochronology. Journal of Volcanology and Geothermal Research 34, 153–172.

Pelle, T., Scarciglia, F., Allevato, E., Di Pasquale, G., La Russa, M.F., Marino, D., Natali, E., Robustelli, G., Tiné, V., 2013a. Reconstruction of Holocene environmental changes in two archaeological sites of Calabria (southern Italy) using an integrated pedological and anthracological approach. Quaternary International 288, 206–214.

Pelle, T., Scarciglia, F., Di Pasquale, G., Allevato, E., Marino, D., Robustelli, G., La Russa, M.F., Pulice, I., 2013b. Multidisciplinary study of Holocene archaeological soils in an upland Mediterranean site: natural versus anthropogenic environmental changes at Cecita Lake, Calabria, Italy. Quaternary International 303, 163–179.

Pellegrino, A., Prestininzi, A., 2007. Impact of weathehering on the geomechanical properties of rocks along thermal-matamorphic contact belts and morpho-evolutionary processes: the deep-seated gravitational slope deformations of Mt. Granieri-Salincriti (Calabria-Italy). Geomorphology 87 (3), 176–195.

Perri, F., Cirrincione, R., Critelli, S., Mazzoleni, P., Pappalardo, A., 2008. Clay mineral assemblages and sandstone compositions of the Mesozoic Longobucco Group, northeastern Calabria. Implications for burial history and diagenetic evolution. International Geology Review 50, 1116–1131.

Perri, F., Borrelli, L., Critelli, S., Gullà, G., 2012a. Investigation of weathering rates and processes affecting plutonic and metamorphic rocks in Sila Massif (Calabria, southern Italy). Rendiconti Online della Società Geologica Italiana 21, 557–559.

Perri, F., Critelli, S., Dominici, R., Muto, F., Tripodi, V., Ceramicola, S., 2012b. Provenance and accommodation pathways of late Quaternary sediments in the deep-water northern Ionian Basin, southern Italy. Sedimentary Geology 280, 244–259.

Perri, F., Borrelli, L., Critelli, S., Gullà, G., 2014. Chemical and minero-petrographic features of Plio-Pleistocene fine-grained sediments in Calabria (southern Italy). Italian Journal of Geosciences 133 (1), 101–115.

Perri, F., Scarciglia, F., Apollaro, C., Marini, L., 2015. Characterization of granitoid profiles in the Sila Massif (Calabria, southern Italy) and reconstruction of weathering processes by mineralogy, chemistry, and reaction path modeling. Journal of Soils and Sediments 15 (6), 1351–1372.

Peters, Tj., Hofmann, B., 1984. Hydrothermal clay mineral formation in a biotite-granite in northern Switzerland. Clay Minerals19, 579–590.

Pope, G.A., 2013a. Weathering and sediment genesis. In: Shroder, J.F. (Ed.), Treatise on geomorphology, vol. 4, chapter 17 – Weathering and soils geomorphology. Academic, Press, San Diego, pp. 284–293.

Pope, G.A., 2013b. Weathering in the Tropics, and related extratropical processes. In: Shroder, J.F. (Ed.), Treatise on geomorphology, vol. 4, chapter 11 – Weathering and soils geomorphology. Academic, Press, San Diego, pp. 179–196.

Power, E.T., Smith, B.J., 1994. A comparative study of deep weathering and weathering products: case studies from Ireland, Corsica and Southeast Brazil. In: Robinson, D.A., Williams, R.B.G. (Eds.), Rock Weathering and Landform Evolution. John Wiley and Sons, New York, pp. 21–40.

Que, M., Allen, A.R., 1996. Sericitization of plagioclase in the Rosses Granite Complex, Co. Donegal, Ireland. Mineralogical Magazine 60, 927–936.

Riebe, C.S., Kirchner, J.W., Granger, D.E., Finkel, R.C., 2001. Strong tectonic and weak climatic control of long-term chemical weathering rates. Geology 29, 511–514.

Reimann, C., Siewers, U., Tarvainen, T., Bityukova, L., Eriksson, J., Gilucis, A., Gregorauskiene, V., Lukashev, V.K., Matinian, N.N., Pasieczna, A., 2003. Agricultural soils in northern Europe: A geochemical atlas. Geologisches Jahrbuch Sonderhefte Reihe D, Heft SD 5, Hannover, 279 pp.

Riebe, C.S., Kirchner, G., Finkel, R.C., 2003. Long-term rates of chemical weathering and physical erosion from cosmogenic nuclides and geochemical mass balance. Geochimica et Cosmochimica Acta 67, 4411–4427.

Ruxton, B.P., Berry, L., 1957. Weathering of granite and associated erosional features in Hong Kong. Geological Society of America Bulletin 68, 1263–1282.

Scarciglia, F., 2015. Weathering and exhumation history of the Sila Massif upland plateaus, southern Italy: a geomorphological and pedological perspective. Journal of Soils and Sediments 15 (6), 1278–1291.

Scarciglia, F., Le Pera, E., Critelli, S., 2005a. Weathering and pedogenesis in the Sila Grande Massif (Calabria, South Italy): from field scale to micromorphology. Catena 61 (1), 1–29.

Scarciglia, F., Le Pera, E., Vecchio, G., Critelli, S., 2005b. The interplay of geomorphic processes and soil development in an upland environment, Calabria, South Italy. Geomorphology 69 (1–4), 169–190.

Scarciglia, F., Le Pera, E., Critelli, S., 2007. The onset of the sedimentary cycle in a mid-latitude upland environment: weathering, pedogenesis, and geomorphic processes on plutonic rocks (Sila Massif, Calabria). In: Arribas, J., Critelli, S., Johnsson, M.J. (Eds.), Sedimentary Provenance and Petrogenesis: Perspectives from Petrography and Geochemistry. Geological Society of America Special Paper 420, pp. 149–166.

Scarciglia, F., De Rosa, R., Vecchio, G., Apollaro, C., Robustelli, G., Terrasi, F., 2008. Volcanic soil formation in Calabria (southern Italy): the Cecita Lake geosol in the late Quaternary geomorphological evolution of the Sila uplands. Journal of Volcanology and Geothermal Research 177 (1), 101–117.

Scarciglia, F., Tuccimei, P., Vacca, A., Barca, D., Pulice, I., Salzano, R., Soligo, M., 2011. Soil genesis, morphodynamic processes and chronological implications in two soil transects of SE Sardinia, Italy: traditional pedological study coupled with laser ablation ICP-MS and radionuclide analyses. Geoderma 162 (1-2), 39–64.

Scarciglia, F., Saporito, N., La Russa, M.F., Le Pera, E., Macchione, M., Puntillo, D., Crisci, G.M., Pezzino, A., 2012. Role of lichens in weathering of granodiorite in the Sila uplands (Calabria, southern Italy). Sedimentary Geology 280, 119–134.

Scarciglia, F., Pelle, T., Pulice I., Robustelli, G., 2015. A comparison of Quaternary soil chronosequences from the Ionian and Tyrrhenian coasts of Calabria, southern Italy: Rates of soil development and geomorphic dynamics. Quaternary International 376, 146–162.

Schiattarella, M., Di Leo, P., Beneduce, P., Giano, S.I., Martino C., 2006. Tectonically driven exhumation of a young orogen: an example from southern Apennines, Italy. In: Willett S.D., Hovius, N., Brandon, M.T., Fisher, D. (Eds.), Tectonics, climate, and landscape evolution. Geological Society of America, Special Paper 398, Penrose Conference Series, 371–385.

Schiattarella, M., Giano, S.I., Gioia, D., Martino, C., Nico, G., 2013. Age and statistical properties of the summit paleosurface of southern Italy. Geografia Fisica e Dinamica Quaternaria 36 (2), 289–302.

Sequeira Braga, M.A., Paquet, H., Begonia, A., 2002. Weathering of granites in a temperate climate (NW Portugal): granitic saprolites and arenization. Catena 49, 41–56.

Spina, V., Galli, P., Tondi, E., Critelli, S., Cello, G., 2007. Kinematics and structural properties of an active fault zone in the Sila Massif (Northern Calabria, Italy). Bollettino della Società Geologica Italiana 126 (2), 427–438.

Spina, V., Tondi, E., Mazzoli, S., 2011. Complex basin development in a wrench-dominated back-arc area: Tectonic evolution of the Crati Basin, Calabria, Italy. Journal of Geodynamics 51, 90–109.

Stoops, G., ., Marcelino, V., Mees, F., 2010. Micromorphological features and their relation to processes and classification: general guidelines and keys. In: Stoops, G., Marcelino, V., Mees, F. (Eds), Interpretation of micromorphological features of soils and regoliths. Elsevier, Amsterdam, pp. 15–35.

Suresh, P.O., Dosseto, A., Hesse, P.P., Handley, H.K., 2013. Soil formation rates determined from Uranium-series isotope disequilibria in soil profiles from the southeastern Australian highlands. Earth and Planetary Science Letters 379, 26–37.

Taboada, T., García, C., 1999a. Pseudomorphic transformation of plagioclases during the weathering of granitic rocks in Galicia (NW Spain): Catena 35, 291–302.

Taboada, T, García, C., 1999b. Smectite formation produced by weathering in a coarse granite saprolite in Galicia (NW Spain). Catena 35, 281–290.

Tansi, C., Muto, F., Critelli, S., Iovine, G., 2007. Neogene-Quaternary strike-slip tectonics in the central Calabrian Arc (Southern Italy). Journal of Geodynamics 43, 393–414.

Targulian, V.O., Krasilnikov, P.V., 2007. Soil system and pedogenic processes: self organization, time scales, and environmental significance. Catena 71, 373–381.

Teeuw, R.M., Thomas, M.F., Thorp, M.B., 1994. Regolith and landscape development in the Koidu basin of Sierra Leone. In: Robinson, D.A., Williams, R.B.G. (Eds.), Rock Weathering and Landform Evolution. Wiley, New York, pp. 303–320.

Terranova, O., Antronico, L., Coscarelli, R., Iaquinta, P., 2009. Soil erosion risk scenarios in the Mediterranean environment using RUSLE and GIS: An application model for Calabria (southern Italy). Geomorphology 112, 228–245.

Terranova, O., Antronico, L., Gullà, G., 2007. Landslide triggering scenarios in homogeneous geological contexts: The area surrounding Acri (Calabria, Italy). Geomorphology 87, 250–267.

Thomson, S.N., 1998. Assessing the nature of tectonic contacts using fission-track thermochronology: an example from the Calabrian Arc, southern Italy. Terra Nova 10 (1), 32–36.

Tortorici, L., Monaco, C., Tansi, C., Cocina, O., 1995. Recent and active tectonics in the Calabrian arc (Southern Italy). Tectonophysics 243, 37–55.

Tripodi, V., Muto, F., Critelli, S., 2013. Structural style and tectonostratigraphic evolution of the Neogene-Quaternary Siderno Basin, southern Calabrian Arc, Italy. International Geology Review 4,468–481.

Tyler, G., 2004. Vertical distribution of major, minor, and rare elements in a Haplic Podzol. Geoderma 119, 277–290.

Van Dijk, J.P., Bello, M., Brancaleoni, G.P., Cantarella, G., Costa, V., Frixa, A., Golfetto, F., Merlini, S., Riva, M., Torricelli, S., Toscano, C., Zerilli, A., 2000. A regional structural model for the northern sector of the Calabrian Arc (southern Italy).Tectonophysics 324, 267–320.

Viles, H.A., 2001. Scale issues in weathering studies. Geomorphology 41, 63–72.

Viles, H.A., 2013. Synergistic weathering processes. In: Shroder, J.F. (Ed.), Treatise on geomorphology, vol. 4, chapter 2 – Weathering and soils geomorphology. Academic, Press, San Diego, pp. 12–26.

Vingiani, S., Scarciglia, F., Mileti, F.A., Donato, P., Terribile, F., 2014. Occurrence and origin of soils with andic properties in Calabria (southern Italy). Geoderma, 232–234, 500–516.

von Eynatten, H., Tolosana-Delgado, R., Karius, V., Bachmann, K., Caracciolo, L., 2016. Sediment Generation in humid Mediterranean setting: Grain-size and Source-rock control on sediment geochemistry and mineralogy (Sila Massif, Calabria). Sedimentary Geology, in press. doi: 10.1016/j.sedgeo.2015.10.008

Wan, S., Clift, P.D., Li., A, Li, T., Yin, X., 2010. Geochemical records in the South China Sea: implications for East Asian summer monsoon evolution over the last 20 Ma. In: Clift, P. D., Tada, R., Zheng, H. (Eds.), Monsoon Evolution and Tectonics–Climate Linkage in Asia. Geological Society, London, Special Publication 342, 245–263.

Wennrich, V., Minyuk, P.S., Borkhodoev, V., Francke, A., Ritter, B., Nowaczyk, N.R., Sauerbrey, M.A., Brigham-Grette, J., Melles, M., 2014. Pliocene to Pleistocene climate and environmental history of Lake El'gygytgyn, Far East Russian Arctic, based on high-resolution inorganic geochemistry data. Climate of the Past 10, 1381–1399.

Westaway, R., 1993. Quaternary uplift of southern Italy. Journal of Geophysical Research 98, 21741–21772.

White, A.F., 2005. Natural weathering rates of silicate minerals. In: Drever, J.I. (Ed.), Surface and ground water, weathering, and soils, Treatise on geochemistry (Holland, H.D., Turekian, K.K., Eds.), vol. 5, chapter 6, Elsevier–Pergamon, Oxford, pp. 133–168.

Zauyah, S., Schaefer, C.E.G.R., Simas, F.N.B., 2010. Saprolites. In: Stoops, G., Marcelino, V., Mees, F. (Eds), Interpretation of micromorphological features of soils and regoliths. Elsevier, Amsterdam, pp. 49–68.

Zecchin, M., Caffau, M., Civile, D., Critelli, S., Di Stefano, A., Maniscalco, R., Muto, F., Sturiale, G., Roda, C., 2012. The Plio-Pleistocene evolution of the Crotone Basin (southern Italy): interplay between sedimentation, tectonics and eustasy in the frame of Calabrian Arc migration. Earth-Science Reviews 115 (4), 273–303.

Figure captions

Fig. 1. Location map of the study area.

Fig. 2. A) Geological and structural sketch map of the study area: 1) Holocene deposits; 2) Plio-Pleistocene deposits; 3) Miocene deposits; 4) Mesozoic sedimentary cover; 5) plutonic rocks (Sila batholith; Carboniferous-Permian); 6) high-grade metamorphic rocks; 7) low- to medium-grade metamorphic rocks; 8) normal faults; 9) strike-slip faults; 10) major fractures. B) Map of the weathering macro-classes referred to granitoid rocks and the main tectonic lineaments.

Fig. 3. Field examples of complex weathering patterns in the study area: A) Abrupt change between weathering classes III and V separated by a subvertical fault plane (red arrows) near Savelli site; B) juxtaposition of different weathering classes along a fault zone (red arrows) in the Castelsilano area close to Savelli village; C) dyke included in the saprolite, San Giovanni in Fiore site; D) weathering profile showing angular to rounded rock masses and corresponding detritus, which also includes granular material (San Giovanni in Fiore).

Fig. 4. A, B, C: Typical weathering profiles dominated by completely weathered rock (class V) and characterized by increasing depths: A) Acri, B) Castelsilano (Savelli), and C) Savelli site.

Fig. 5. A, B) Spheroidal boulders exhumed at the topographic surface, overlying weathering profiles with different features (Silvana Mansio site). C) Slightly weathered granodiorite rock from a boulder showing partially oxidized and exfoliated biotite crystals (Silvana Mansio); D) Surface exfoliation (red arrows) and lichen cover on a boulder at Silvana Mansio site.

Fig. 6. A) Weathering profile with a typical concentric, spheroidal pattern isolating rounded corestones in the saprolite (Silvana Mansio). B) Completely weathered rock sample affected by centimetric microfractures (red arrows). C) Very shallow soil (ca. 40 cm deep) overlying a highly weathered rock of class IV. D) Typical soil profile overlying the saprolite close to Silvana Mansio.

Fig. 7. A) Detail of a saprolitic mass showing an iron- and clay-rich groundmass, which still includes whitish relicts of the original rock. Illuvial Fe-Mn oxyhydroxide (B) and clay coatings (C, D) on joint surfaces of granodiorite (Silvana Mansio site).

Fig. 8. Microphotographs of thin sections of samples from Acri and San Giovanni in Fiore sites: A) peculiar granite characterized by prevalent microcline crystals (XPL); B) common mineral assemblage of granite including quartz, K-feldspar, plagioclase and biotite (XPL); C) sericitization of the inner core of a

plagioclase grain (XPL); D, E, F) iron-oxide coatings released from weathered biotite grains (red dotted circle) into the surrounding microcracks (red arrows) (PPL); F) close-up of the image in figure 8E; G, H) biotite crystal split along cleavage planes with microcracks radiating into the surrounding mineral grains (red arrows) (PPL, XPL).

Fig. 9. Microphotographs of thin sections of samples from Acri and San Giovanni in Fiore sites: A, B) weathered biotite with release of clay and iron-oxide coatings into surrounding rock microcracks (red arrow) (PPL, XPL); C, D) intensely weathered biotite, in place largely replaced by clays and iron-oxides appearing as matrix patches) (PPL, XPL); E, F) very weathered plagioclase with diffuse surface pitting and local neoformed clay (red circle) and Fe-oxide staining (red arrow) (PPL, XPL); quartz grain affected by outer edge and surface pitting (red arrows) (PPL, XPL).

Fig. 10. SEM images and EDS spectra of fresh (A, C) and weathered parts (B, D) of mica minerals showing argillified flakes in rock samples of classes III-IV and IV-V, respectively (San Giovanni in Fiore area). Red arrows indicate approximate location of microprobe analyses. A and B refer to class III-IV, whereas C and D refer to class IV-V.

Fig. 11. SEM images of rock samples from San Giovanni in Fiore and Silvana Mansio sites: A) weathered plagioclase exhibiting surface argillification and dissolution, coupled with Fe-oxide segregations (red arrow), and corresponding EDS spectrum (class V-VI); B) quartz grain with occasional etch pits (red arrows) and curved to linear, parallel and stepped dissolution features (class IV); C, D) illuvial clay coatings with surface microcracks (red arrows) on rock samples of classes III-IV and V, respectively, and compositional EDS spectra.

Fig. 12. Distribution of CIA values (A) and some molar ratios between relatively immobile major elements, reported as oxides (B-D), according to weathering grade classes.

Fig. 13. Distribution of some major oxides versus TiO_2 according to weathering grade classes (A-D).

Fig. 14. Distribution of Fe_2O_3 versus TiO_2 (A) and some trace elements versus Ti (B-D) according to weathering grade classes.

Fig. 15. Distribution of some trace element ratios according to weathering grade classes (A-D).

Fig. 16. Distribution of some trace element ratios according to weathering grade classes (A-D).

Table captions

Table 1

Weathering grade classes based on morphological criteria and physico-mechanical field tests.
Based on Gullà and Matano (1997); modified after Borrelli et al. (2014b).
$N_{Schmidt}$: rebound value obtained with a Schmidt hammer.

Table 2

Values obtained for the micropetrographic index (Ip) proposed by Irfan and Dearman (1978).
SGF: San Giovanni in Fiore.

Table 3

Mean values of major element concentrations (expressed as weight percent of oxides) and chemical index of alteration (CIA; Nesbitt and Young, 1982) for each weathering grade class.
*: data from Messina et al. (1991). St. dev.: standard deviation.

Table 4

Mean values of trace element concentrations (expressed in mg kg^{-1}) for each weathering grade class.
*: data from Messina et al. (1991); St. dev.: standard deviation; b.d.l.: below detection limits.

Table 5

Soil formation rates calculated for soil horizons, saprolitic layers and less weathered rock samples of the weathering profile. See text for more details.

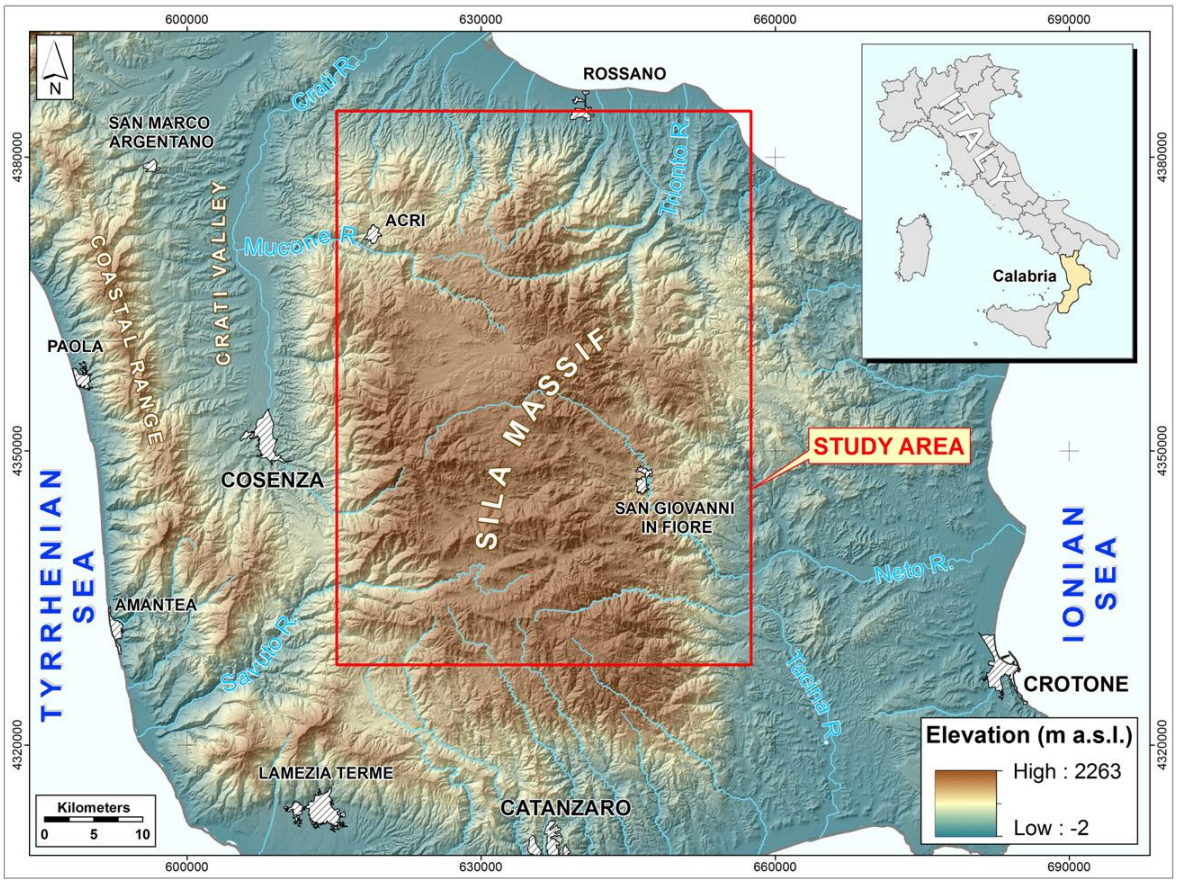
600000
630000
660000
690000
4380000
4350000
4320000
N
ROSSANO
SAN MARCO ARGENTANO
Crati R.
Trionto R.
ACRI
Mucone R.
COASTAL RANGE
CRATI VALLEY
PAOLA
SILA MASSIF
STUDY AREA
COSENZA
SAN GIOVANNI IN FIORE
TYRRHENIAN SEA
IONIAN SEA
AMANTEA
Savuto R.
Neto R.
Tacina R.
CROTONE
LAMEZIA TERME
CATANZARO
ITALY
Calabria
Kilometers
0 5 10
Elevation (m a.s.l.)
High : 2263
Low : -2

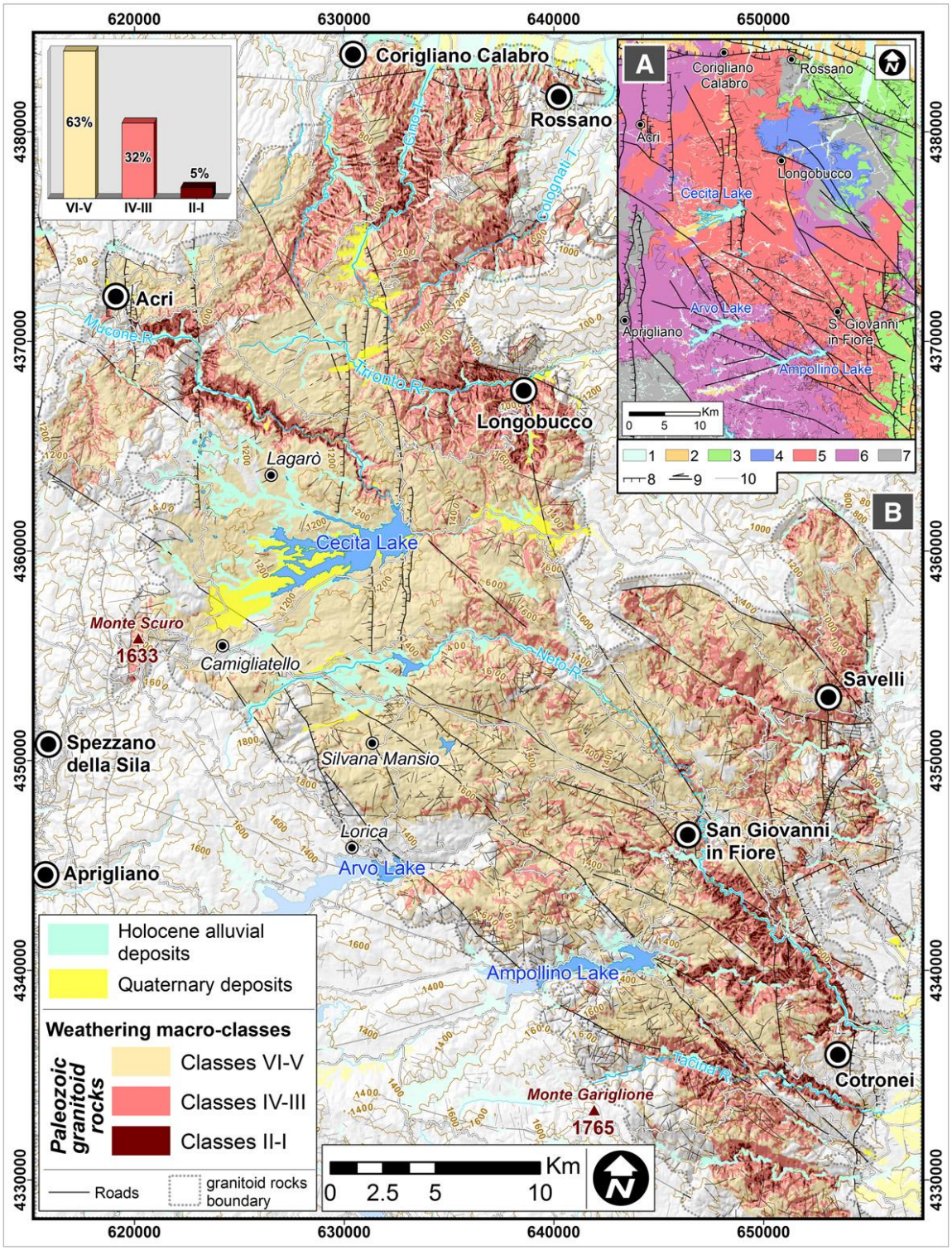
620000
630000
640000
650000
4380000
4370000
4360000
4350000
4340000
4330000
Corigliano Calabro
Rossano
Acri
Longobucco
Lagarò
Cecita Lake
Monte Scuro
1633
Camigliatello
Spezzano della Sila
Silvana Mansio
Lorica
Arvo Lake
Apprigliano
Savelli
San Giovanni in Fiore
Ampollino Lake
Cotronei
Monte Gariglione
1765
Mucone R.
Trionto R.
Neto R.
Coscile T.
Crati R.
Tacina R.
63%
32%
5%
VI-V
IV-III
II-I
A
B
Km
0 5 10
1 2 3 4 5 6 7
8 9 10
Holocene alluvial deposits
Quaternary deposits
Weathering macro-classes
Paleozoic granitoid rocks
Classes VI-V
Classes IV-III
Classes II-I
Roads
granitoid rocks boundary
0 2.5 5 10

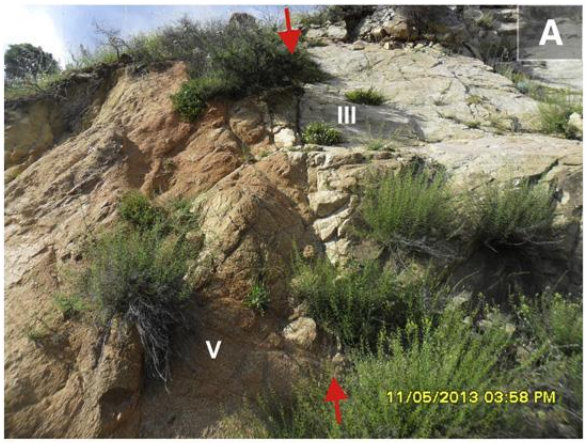
A
III
V
11/05/2013 03:58 PM


B
V
V-IV
III
11/05/2013 03:55 PM


C
V


D
IV-III
IV
V
V
IV


A


B
11/05/2013 11:52 AM


C


A
B
C
D

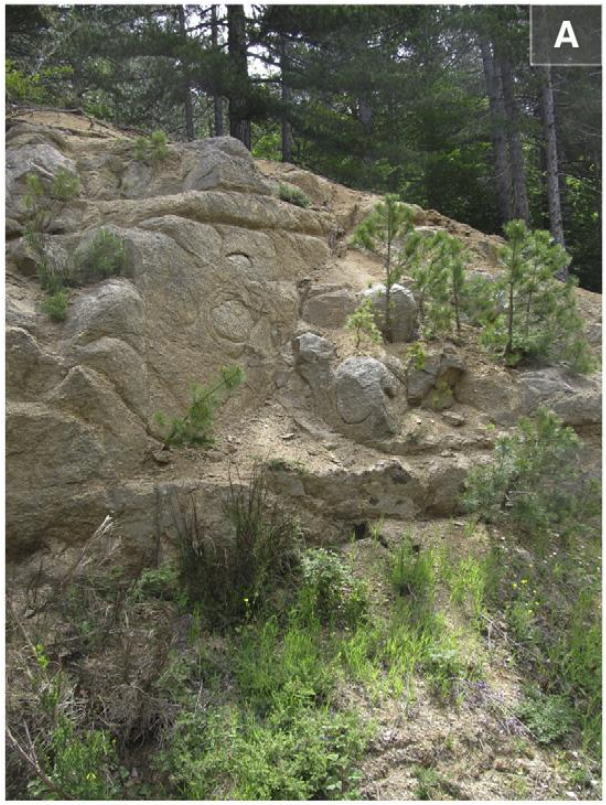
A

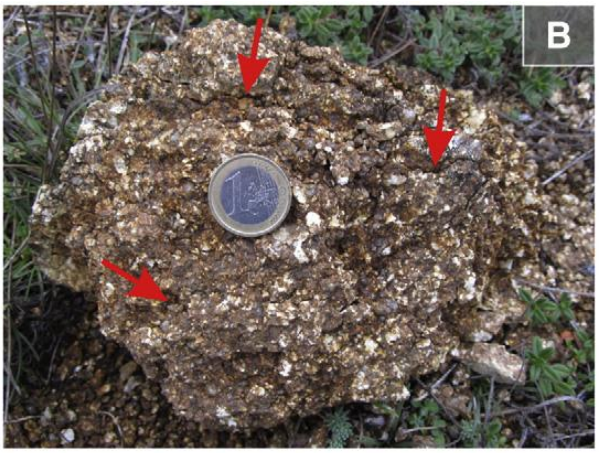
B


C


D

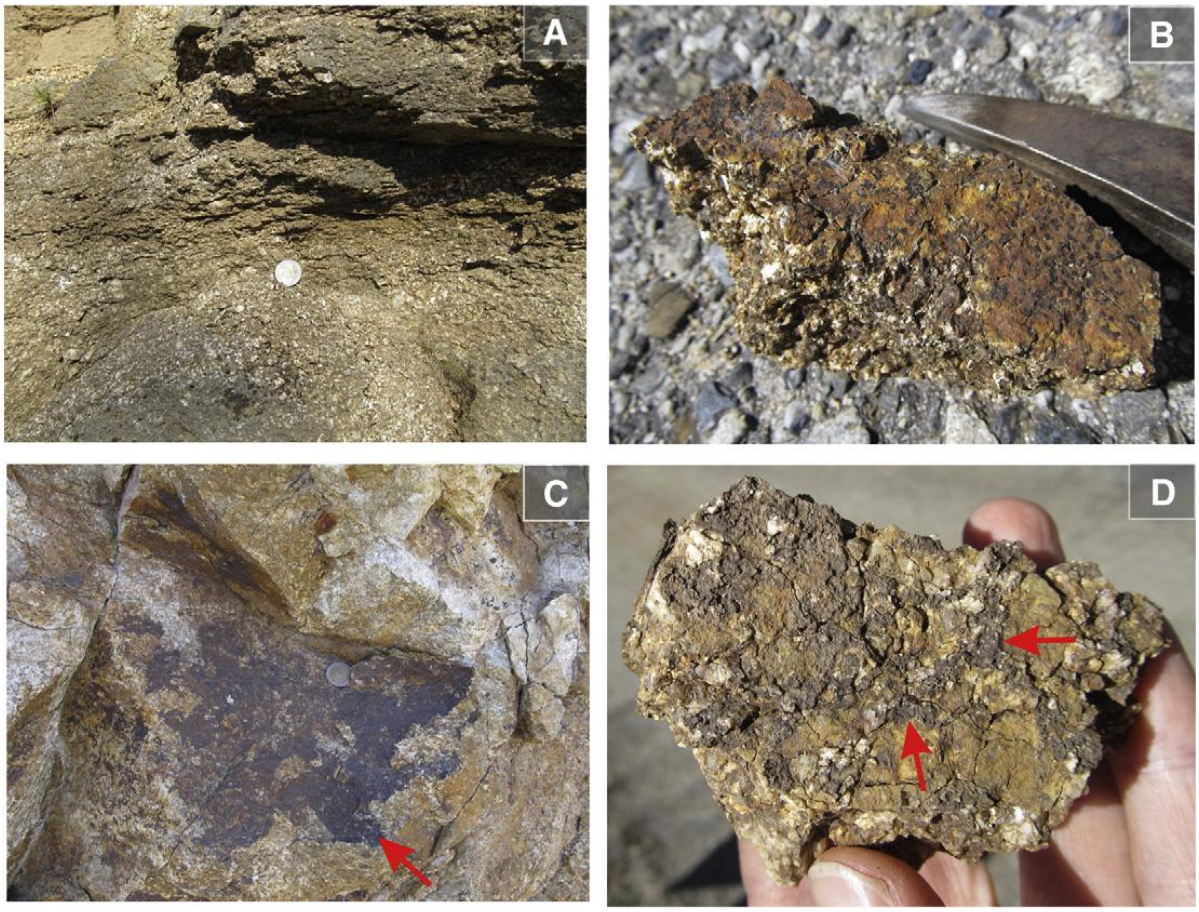
A
B
C
D

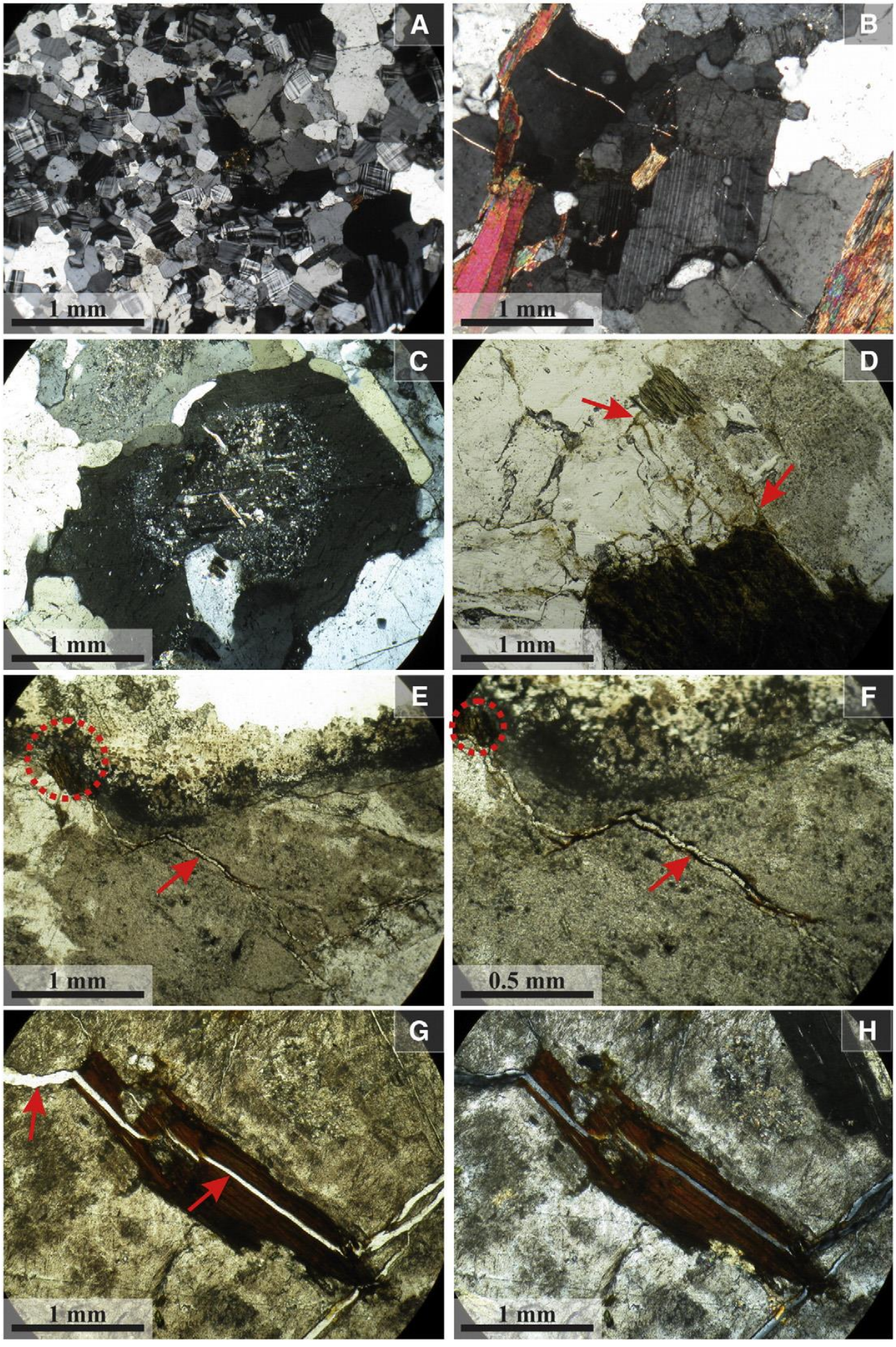
A
1 mm
B
1 mm
C
1 mm
D
1 mm
E
1 mm
F
0.5 mm
G
1 mm
H
1 mm

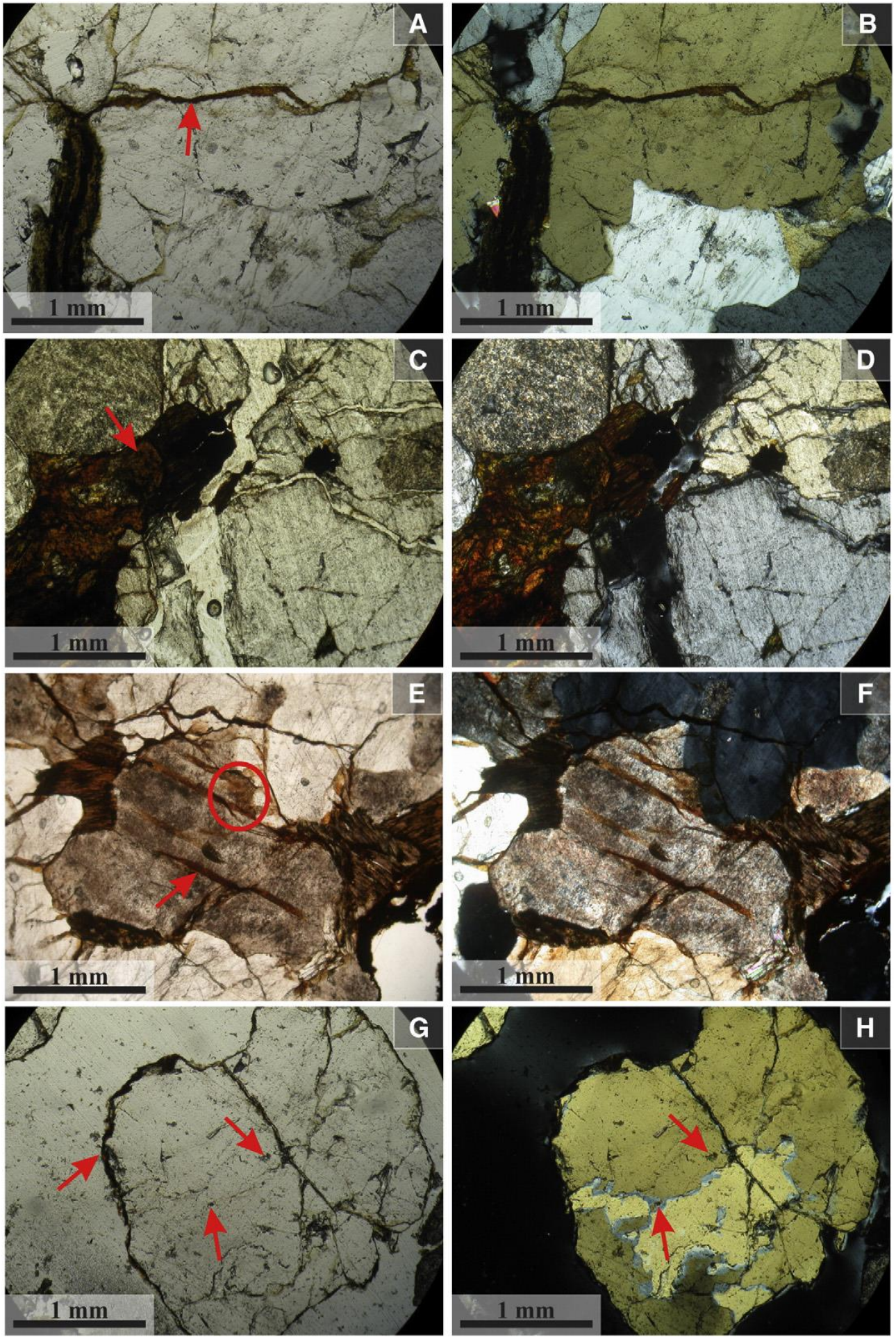
A
1 mm
B
1 mm
C
1 mm
D
1 mm
E
1 mm
F
1 mm
G
1 mm
H
1 mm

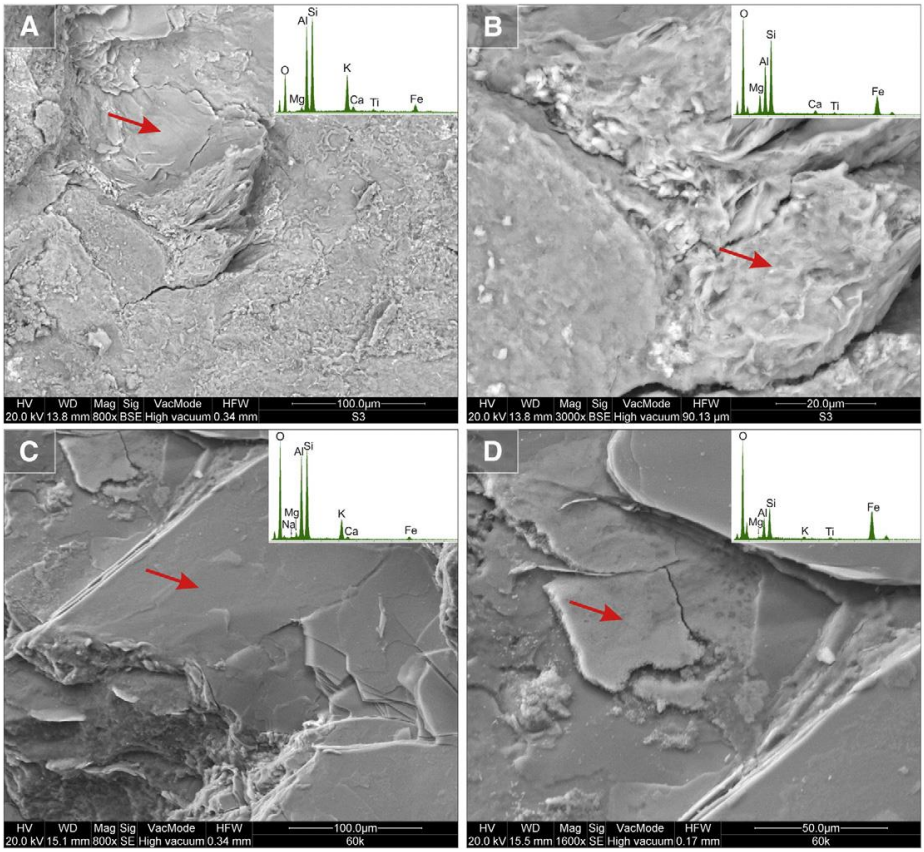
A
Si
Al
O
K
Mg
Ca
Ti
Fe
HV WD Mag Sig VacMode HFW
20.0 kV 13.8 mm 800x BSE High vacuum 0.34 mm
100.0µm
S3
B
O
Si
Al
Mg
Ca
Ti
Fe
HV WD Mag Sig VacMode HFW
20.0 kV 13.8 mm 3000x BSE High vacuum 90.13 µm
20.0µm
S3
C
O
Al
Si
Mg
Na
K
Ca
Fe
HV WD Mag Sig VacMode HFW
20.0 kV 15.1 mm 800x SE High vacuum 0.34 mm
100.0µm
60k
D
O
Si
Al
Mg
Fe
K
Ti
HV WD Mag Sig VacMode HFW
20.0 kV 15.5 mm 1600x SE High vacuum 0.17 mm
50.0µm
60k

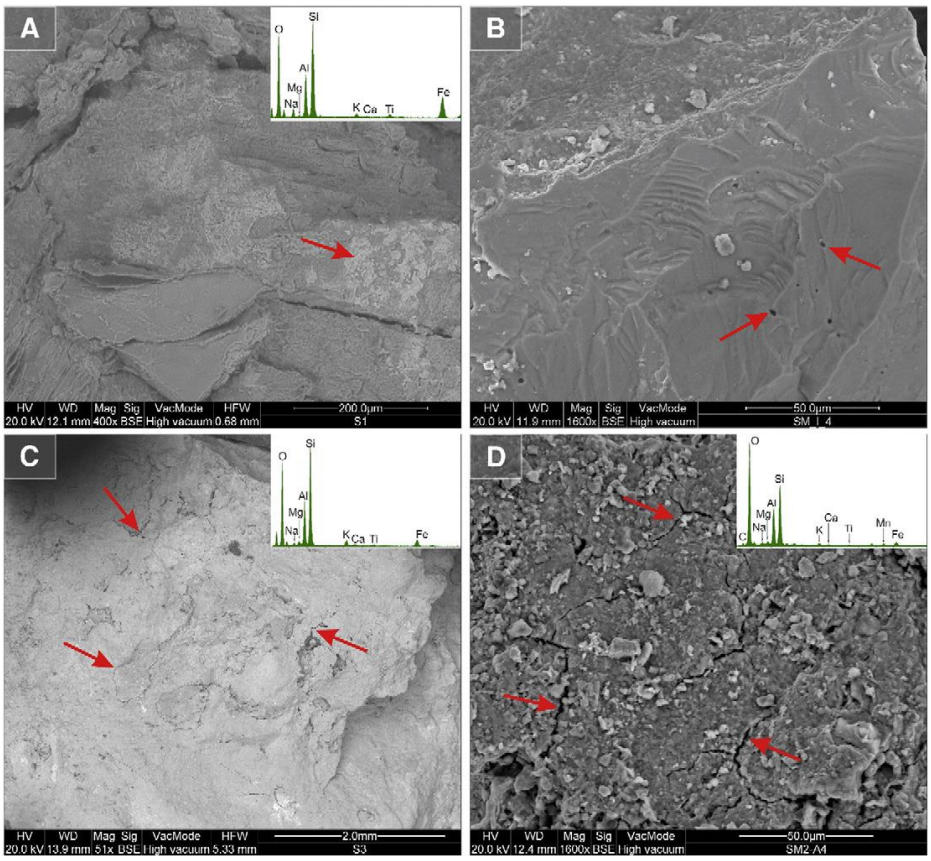
A
Si
O
Al
Mg
Na
K
Ca
Ti
Fe
HV WD Mag Sig VacMode HFW
20.0 kV 12.1 mm 400x BSE High vacuum 0.68 mm
200.0µm
S1
B
HV WD Mag Sig VacMode
20.0 kV 11.9 mm 1600x BSE High vacuum
50.0µm
SM_I_4
C
Si
O
Al
Mg
Na
K
Ca
Ti
Fe
HV WD Mag Sig VacMode HFW
20.0 kV 13.9 mm 51x BSE High vacuum 5.33 mm
2.0mm
S3
D
O
Si
Al
Mg
Na
C
Ca
K
Ti
Mn
Fe
HV WD Mag Sig VacMode
20.0 kV 12.4 mm 1600x BSE High vacuum
50.0µm
SM2-A4

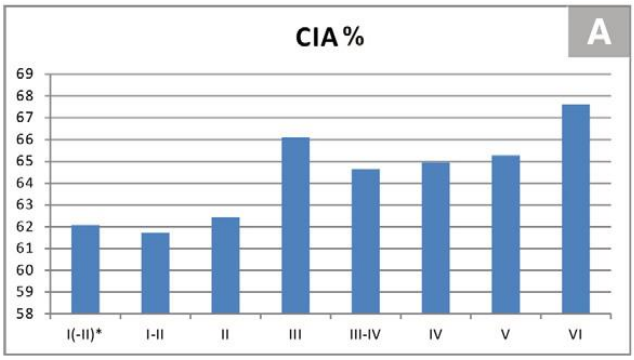
CIA %
A
69
68
67
66
65
64
63
62
61
60
59
58
I(-II)*
I-II
II
III
III-IV
IV
V
VI

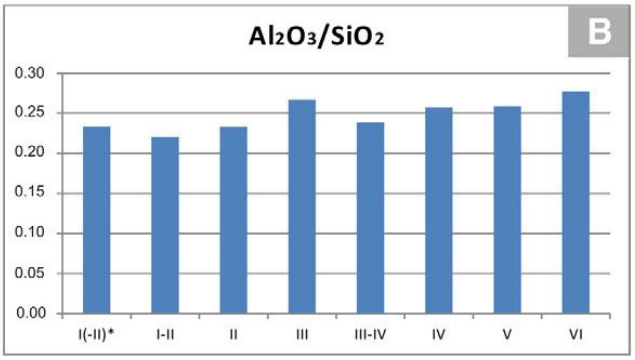
Al2O3/SiO2
B
0.30
0.25
0.20
0.15
0.10
0.05
0.00
I(-II)*
I-II
II
III
III-IV
IV
V
VI

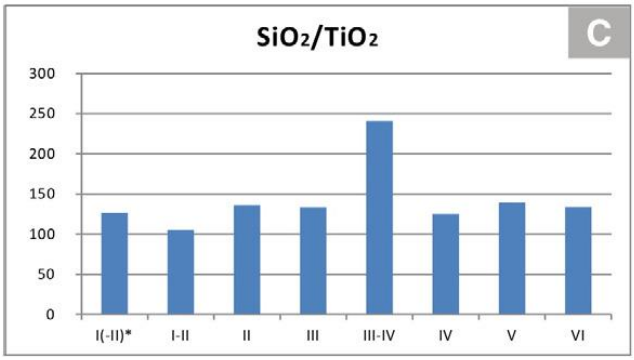
SiO2/TiO2
C
300
250
200
150
100
50
0
I(-II)*
I-II
II
III
III-IV
IV
V
VI

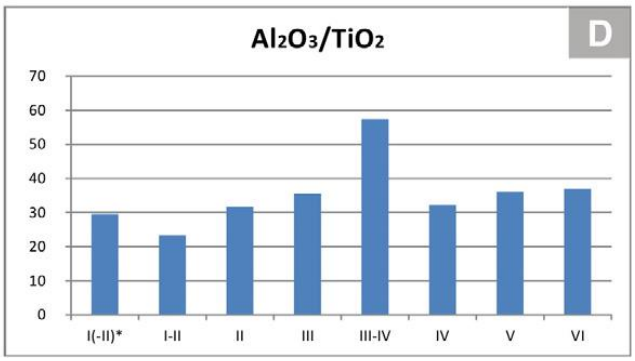
Al2O3/TiO2
D
70
60
50
40
30
20
10
0
I(-II)*
I-II
II
III
III-IV
IV
V
VI

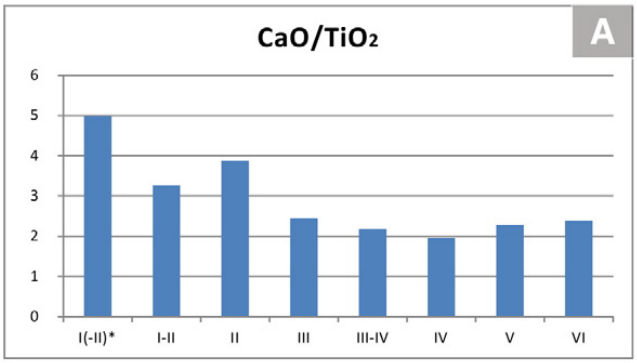
CaO/TiO2
A
6
5
4
3
2
1
0
I(-II)*
I-II
II
III
III-IV
IV
V
VI

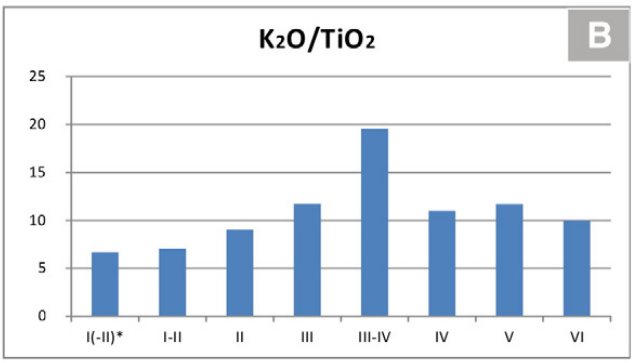
K2O/TiO2
B
25
20
15
10
5
0
I(-II)*
I-II
II
III
III-IV
IV
V
VI

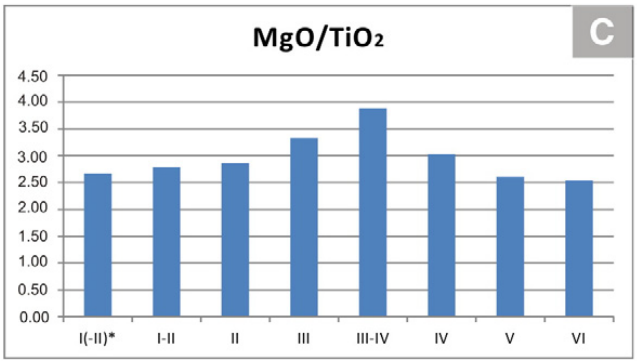
MgO/TiO2
C
4.50
4.00
3.50
3.00
2.50
2.00
1.50
1.00
0.50
0.00
I(-II)*
I-II
II
III
III-IV
IV
V
VI

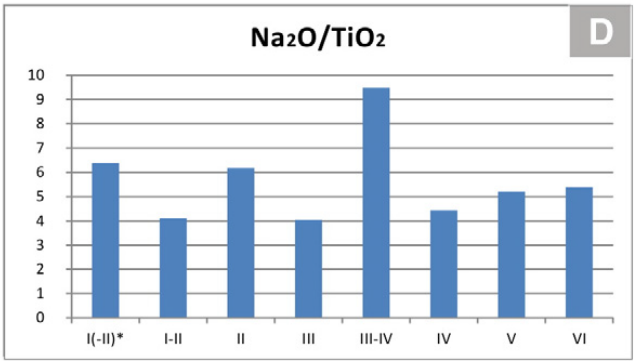
Na2O/TiO2
D
10
9
8
7
6
5
4
3
2
1
0
I(-II)*
I-II
II
III
III-IV
IV
V
VI

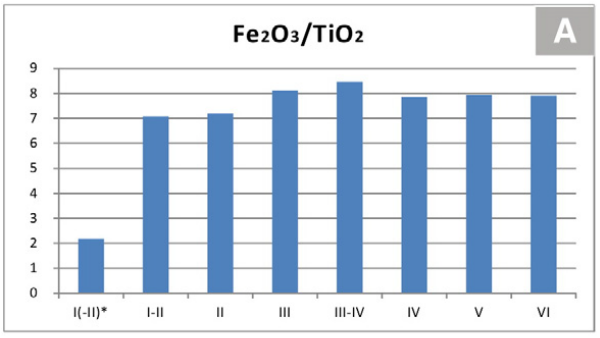
Fe2O3/TiO2
A
9
8
7
6
5
4
3
2
1
0
I(-II)*
I-II
II
III
III-IV
IV
V
VI

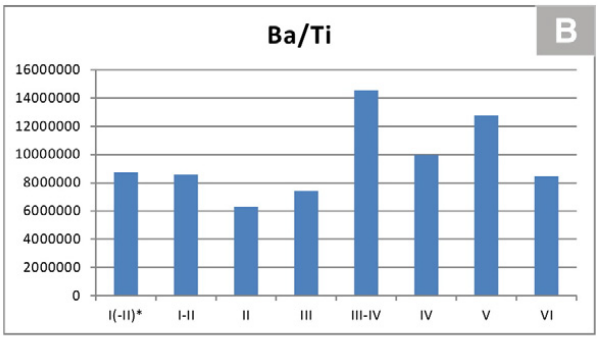
Ba/Ti
B
16000000
14000000
12000000
10000000
8000000
6000000
4000000
2000000
0
I(-II)*
I-II
II
III
III-IV
IV
V
VI

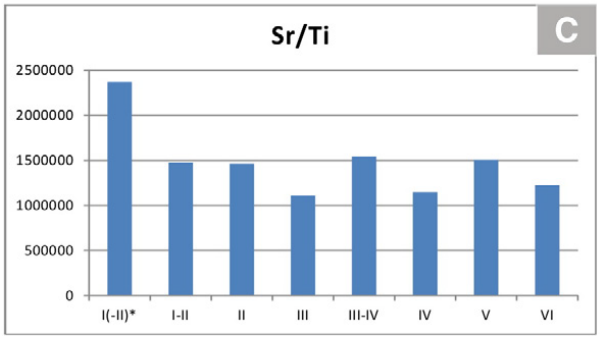
Sr/Ti
C
2500000
2000000
1500000
1000000
500000
0
I(-II)*
I-II
II
III
III-IV
IV
V
VI

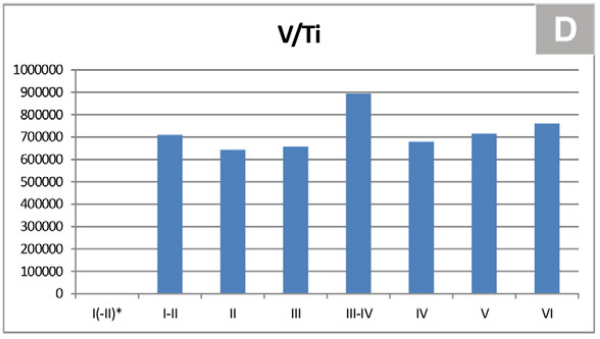
V/Ti
D
1000000
900000
800000
700000
600000
500000
400000
300000
200000
100000
0
I(-II)*
I-II
II
III
III-IV
IV
V
VI

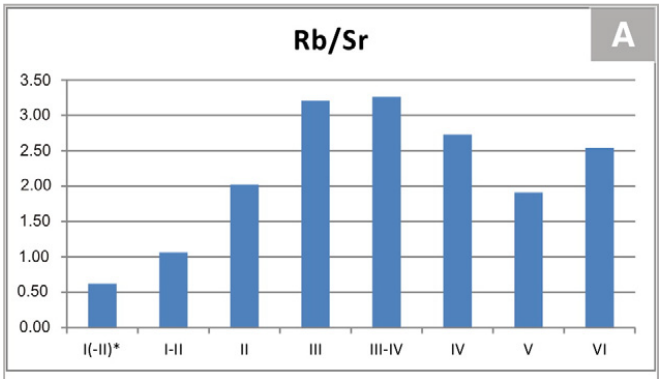
Rb/Sr
A
3.50
3.00
2.50
2.00
1.50
1.00
0.50
0.00
I(-II)*
I-II
II
III
III-IV
IV
V
VI

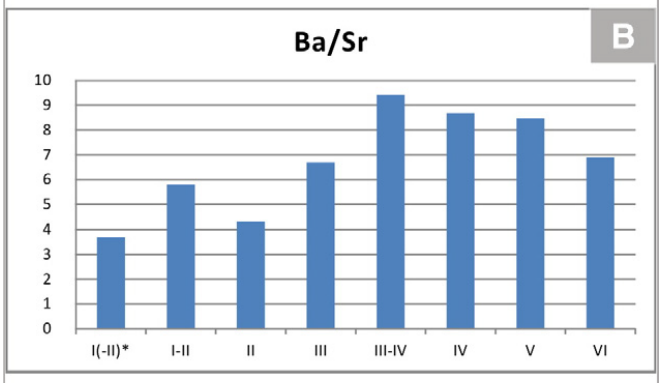
Ba/Sr
B
10
9
8
7
6
5
4
3
2
1
0
I(-II)*
I-II
II
III
III-IV
IV
V
VI

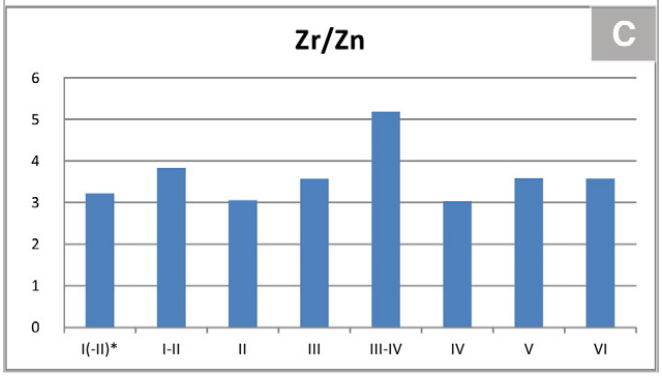
Zr/Zn
C
6
5
4
3
2
1
0
I(-II)*
I-II
II
III
III-IV
IV
V
VI

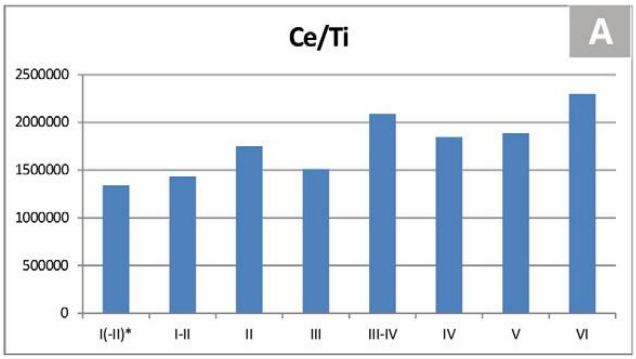

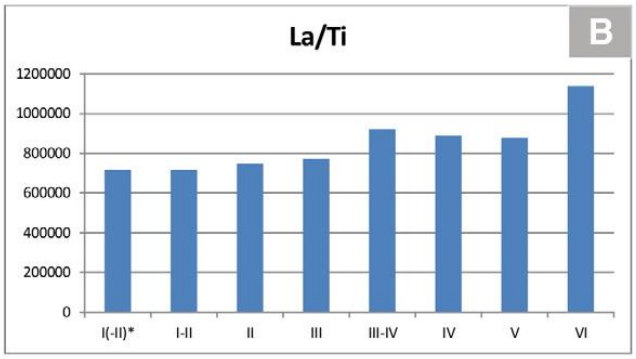

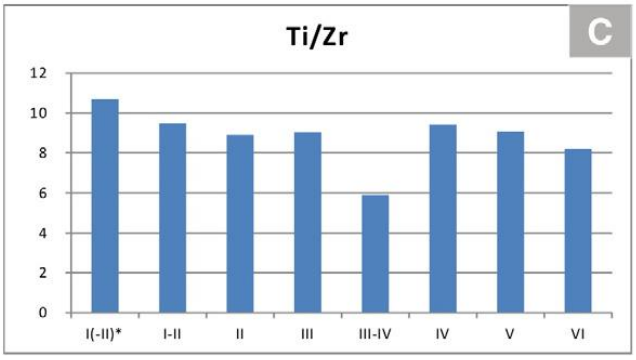

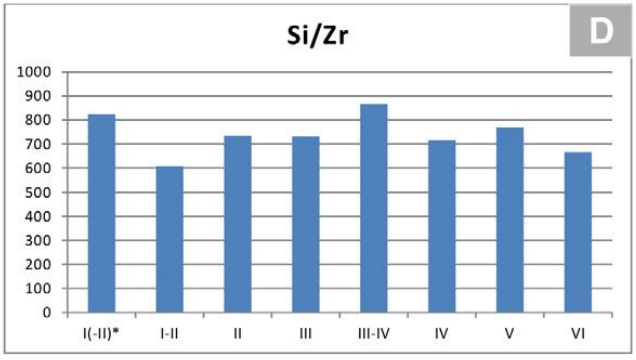

CLASS	ROCK MASS	ROCK MATERIAL
I - Fresh	The rock mass is fresh (more than 70% of the outcrop); limited and isolated rock mass volumes, near the discontinuities, may consist of slightly weathered rock.	No visible signs of weathering on rock mass or slight changes in color (staining) only along major joints.
II – Slightly weathered	The rock mass is slightly weathered (more than 70% of the outcrop); limited and isolated rock mass volumes, near the discontinuities, may consist of moderately weathered rock.	The rock material has mainly the following characteristics: same color of the fresh rock (Class I) with some changes in color only near the discontinuities; original texture and microstructure of the fresh rock are perfectly preserved; strength is comparable to that of the fresh rock (hard rock); rock makes a ringing sound when it is struck by hammer. $N_{Schmidt}$ value > 50.
III - Moderately weathered	The rock mass is moderately weathered (more than 70% of the outcrop); limited and isolated rock mass volumes may consist of highly to slightly weathered rock.	The rock material has mainly the following characteristics: pervasive change in color, although the color of the fresh rock can be present in places; original texture and microstructure of the fresh rock are well preserved; strength is comparable to that of the fresh rock (hard rock); rock makes an intermediate sound when it is struck by hammer; large pieces are hardly broken if it is struck by hammer head; the tip of a geological hammer produces a scratch on the rock surface. $N_{Schmidt}$ value: 25-50.
IV - Highly weathered	The rock mass is highly weathered (more than 70% of the outcrop); limited and isolated rock mass volumes may consist of moderately to completely weathered rock.	The rock material has mainly the following characteristics: pervasive and complete change in color; original texture and microstructure of the fresh rock are still preserved; strength is substantially reduced (weak rock); rock makes an intermediate dull sound when it is struck by hammer; large pieces are easily broken if they are struck by hammer; large pieces do not slake in water; the tip of a geological hammer indents the rock superficially; knife edge produces a scratch on the surface of rock. $N_{Schmidt}$ value: 10-25.
V - Completely weathered	The rock mass is completely weathered (saprolite) (more than 70% of the outcrop); limited and isolated rock mass volumes may consist of completely weathered rock or soil material.	The rock material has mainly the following characteristics: complete change in color; original texture and microstructure of the fresh rock are present in relict form; strength is extremely reduced (soft rock or soil-like behavior); large pieces can be broken by hand and slake in water; the tip of a geological hammer indents the rock deeply; knife edge easily carves the surface of rock; gravel and sand fractions prevail. $N_{Schmidt}$ value: 0-15.
VI – Soil and colluvial material	The rock mass mainly consists of soils and colluvial materials (more than 70% of the outcrop); limited and isolated portions may consist of moderately to highly weathered rock and/or saprolitic material.	The rock material has mainly the following characteristics: all rock material converted to soil; complete change in color; original texture and microstructure of the fresh rock are completely destroyed; development of pedogenetic structure and frequent accumulation of organic matter; large pieces can be easily broken by hand and crumbled by finger pressure into constituent grains. Dominant coarse texture (sand and silt fractions). Colluvial materials, usually located on slopes, footslopes and in morphological depressions, mainly consist of sandy-silty to gravelly chaotic deposits, including moderately to highly weathered, centimetric to decimetric rock fragments.

Weathering grade class	Sample	Location	Unweathered minerals %	Weathered minerals %	Microfractures and voids %	Ip
I-II	C102	Acri	91.83	7.92	0.25	11.24
II	C57	Acri	89.20	9.56	0.52	8.26
II-III	C2	Longobucco	86.00	14.00	0	6.14
II-III	C4	Longobucco	81.00	15.44	3.56	4.26
III	C64	Acri	80.96	16.29	2.75	4.25
III	C103	Acri	82.35	14.58	3.07	4.67
III-IV	SAD	SGF	54.00	35.50	10.50	1.17
III-IV	PT	SGF	19.30	13.50	2.90	1.20
IV-V	S17	SGF	51.50	35.30	13.00	1.07
IV-V	S3	SGF	46.20	39.30	14.50	0.85
IV-V	SA1	SGF	30.60	40.60	27.90	0.40
IV-V	S3 bis	SGF	42.50	46.50	9.90	0.80
IV-V	C1	Longobucco	49.00	49.25	1.75	0.96
IV-V	C3	Longobucco	51.00	38.10	10.09	1.04
IV-V	C8	Longobucco	49.00	49.97	1.03	0.96
IV-V	C9	Longobucco	52.00	41.86	6.14	1.08
V	C60	Acri	64.13	19.14	16.73	1.79
V	C72	Acri	61.20	32.68	6.12	1.57
V	C89	Acri	59.05	29.14	11.81	1.44
V	C104	Acri	42.83	36.20	20.97	0.75
V	SF	SGF	37.70	45.60	16.8	0.6
V-VI	C74	Acri	21.29	64.84	13.87	0.27
V-VI	C77	Acri	42.17	43.77	14.06	0.73
V-IV	C105	Acri	69.20	23.15	7.65	2.24
V-VI	S4	SGF	39.60	48.10	12.00	0.65
V-VI	SV1	SGF	41.90	40.40	17.40	0.72
V-VI	L4	SGF	17.50	33.20	49.00	0.20
V-VI	S1	SGF	20.60	77.30	9.50	0.20
V-VI	C10	Longobucco	23.00	67.86	9.14	0.19

Weathering grade class	**Na_2O %**	**MgO %**	**Al_2O_3 %**	**SiO_2 %**	**P_2O_5 %**	**K_2O %**	**CaO %**	**TiO_2 %**	**MnO %**	**Fe_2O_3 %**	**CIA %**
I(-II)*	3.38	1.41	15.67	67.21	0.19	3.55	2.64	0.53	0.07	1.16	62
St. dev.	*0.19*	*0.19*	*0.39*	*0.71*	*2.33*	*0.03*	*0.35*	*0.57*	*0.07*	*0.02*	*0.59*
I-II	2.52	1.71	14.31	64.83	0.25	4.33	2.00	0.61	0.06	4.35	62
St. dev.	*0.01*	*0.28*	*1.20*	*6.34*	*0.08*	*0.58*	*1.17*	*0.29*	*0.03*	*1.36*	*3.57*
II	2.97	1.38	15.27	65.55	0.24	4.36	1.87	0.48	0.05	3.47	62
St. dev.	*0.51*	*0.61*	*0.76*	*4.38*	*0.09*	*1.49*	*1.12*	*0.25*	*0.04*	*1.84*	*1.32*
III	1.96	1.61	17.20	64.40	0.24	5.66	1.19	0.48	0.05	3.92	66
St. dev.	*0.81*	*0.44*	*2.33*	*3.77*	*0.08*	*1.87*	*0.79*	*0.20*	*0.03*	*1.33*	*1.93*
III-IV	2.68	1.10	16.23	68.08	0.17	5.53	0.62	0.28	0.02	2.39	65
St. dev.	*0.88*	*0.88*	*1.90*	*4.00*	*0.06*	*0.17*	*0.06*	*0.14*	*0.01*	*1.44*	*4.93*
IV	2.26	1.55	16.43	63.87	0.20	5.62	1.00	0.51	0.06	4.01	65
St. dev.	*0.82*	*0.43*	*0.60*	*2.06*	*0.04*	*2.05*	*0.36*	*0.10*	*0.03*	*0.75*	*2.44*
V	2.36	1.18	16.31	63.00	0.17	5.30	1.03	0.45	0.06	3.59	65
St. dev.	*0.35*	*0.19*	*0.82*	*3.18*	*0.06*	*0.62*	*0.33*	*0.08*	*0.04*	*0.67*	*2.29*
VI	2.50	1.18	17.24	62.17	0.20	4.65	1.11	0.47	0.06	3.68	68
St. dev.	*0.50*	*0.32*	*1.01*	*4.68*	*0.07*	*0.66*	*0.64*	*0.15*	*0.03*	*1.22*	*1.93*

Weathering grade class	Na_2O %	MgO %	Al_2O_3 %	SiO_2 %	P_2O_5 %	K_2O %	CaO %	TiO_2 %	MnO %	Fe_2O_3 %	CIA %
I(-II)*	3.38	1.41	15.67	67.21	0.19	3.55	2.64	0.53	0.07	1.16	62
St. dev.	*0.19*	*0.19*	*0.39*	*0.71*	*2.33*	*0.03*	*0.35*	*0.57*	*0.07*	*0.02*	*0.59*
I-II	2.52	1.71	14.31	64.83	0.25	4.33	2.00	0.61	0.06	4.35	62
St. dev.	*0.01*	*0.28*	*1.20*	*6.34*	*0.08*	*0.58*	*1.17*	*0.29*	*0.03*	*1.36*	*3.57*
II	2.97	1.38	15.27	65.55	0.24	4.36	1.87	0.48	0.05	3.47	62
St. dev.	*0.51*	*0.61*	*0.76*	*4.38*	*0.09*	*1.49*	*1.12*	*0.25*	*0.04*	*1.84*	*1.32*
III	1.96	1.61	17.20	64.40	0.24	5.66	1.19	0.48	0.05	3.92	66
St. dev.	*0.81*	*0.44*	*2.33*	*3.77*	*0.08*	*1.87*	*0.79*	*0.20*	*0.03*	*1.33*	*1.93*
III-IV	2.68	1.10	16.23	68.08	0.17	5.53	0.62	0.28	0.02	2.39	65
St. dev.	*0.88*	*0.88*	*1.90*	*4.00*	*0.06*	*0.17*	*0.06*	*0.14*	*0.01*	*1.44*	*4.93*
IV	2.26	1.55	16.43	63.87	0.20	5.62	1.00	0.51	0.06	4.01	65
St. dev.	*0.82*	*0.43*	*0.60*	*2.06*	*0.04*	*2.05*	*0.36*	*0.10*	*0.03*	*0.75*	*2.44*
V	2.36	1.18	16.31	63.00	0.17	5.30	1.03	0.45	0.06	3.59	65
St. dev.	*0.35*	*0.19*	*0.82*	*3.18*	*0.06*	*0.62*	*0.33*	*0.08*	*0.04*	*0.67*	*2.29*
VI	2.50	1.18	17.24	62.17	0.20	4.65	1.11	0.47	0.06	3.68	68
St. dev.	*0.50*	*0.32*	*1.01*	*4.68*	*0.07*	*0.66*	*0.64*	*0.15*	*0.03*	*1.22*	*1.93*

Weathering profile zone	Weathering grade class	Depth (m)	Soil formation rate (mm a^{-1}) estimated for 42 ka	Soil formation rate (mm a^{-1}) estimated for 14 ka
A	VI	0.5	0.01	0.04
Bw	VI	1.0	0.02	0.07
C or Cr	V	1.5	0.04	0.11
C or Cr	V	5.0	0.12	0.36
R	IV to I-II	8.0	0.19	0.57
R	IV to I-II	25.0	0.60	1.79